2017

Fault Location in Transmission Systems Using Synchronized Measurements

Xiangqing Jiao
University of Kentucky, xiangqing.jiao@gmail.com
Digital Object Identifier: https://doi.org/10.13023/ETD.2017.111

STUDENT AGREEMENT:

I represent that my thesis or dissertation and abstract are my original work. Proper attribution has been given to all outside sources. I understand that I am solely responsible for obtaining any needed copyright permissions. I have obtained needed written permission statement(s) from the owner(s) of each third-party copyrighted matter to be included in my work, allowing electronic distribution (if such use is not permitted by the fair use doctrine) which will be submitted to UKnowledge as Additional File.

I hereby grant to The University of Kentucky and its agents the irrevocable, non-exclusive, and royalty-free license to archive and make accessible my work in whole or in part in all forms of media, now or hereafter known. I agree that the document mentioned above may be made available immediately for worldwide access unless an embargo applies.

I retain all other ownership rights to the copyright of my work. I also retain the right to use in future works (such as articles or books) all or part of my work. I understand that I am free to register the copyright to my work.

REVIEW, APPROVAL AND ACCEPTANCE

The document mentioned above has been reviewed and accepted by the student's advisor, on behalf of the advisory committee, and by the Director of Graduate Studies (DGS), on behalf of the program; we verify that this is the final, approved version of the student's thesis including all changes required by the advisory committee. The undersigned agree to abide by the statements above.

Xiangqing Jiao, Student

Dr. Yuan Liao, Major Professor

Dr. Caicheng Lu, Director of Graduate Studies

FAULT LOCATION IN TRANSMISSION SYSTEMS USING SYNCHRONIZED MEASUREMENTS

DISSERTATION

A dissertation submitted in partial fulfillment of the requirements for the degree of Doctor of Philosophy in the College of Engineering at the University of Kentucky

By

Xiangqing Jiao

Lexington, Kentucky

Director: Dr. Yuan Liao, Professor of Electrical and Computer Engineering

Lexington, Kentucky

2017

ABSTRACT OF DISSERATION

FAULT LOCATION IN TRANSMISSION SYSTEMS USING SYNCHRONIZED MEASUREMENTS

Compared with conventional measurements from supervisory control and data acquisition (SCADA) system, phasor measurement units (PMUs) provide time-synchronized and direct measurements of phasors. The availability of synchronized phasor measurements can significantly improve power system protection and analysis. This dissertation is specifically committed to using synchronized measurements for estimation of fault locations in transmission systems.

Transmission lines are prone to various short-circuit faults. Accurate fault location is critical for rapid power recovery. Chapter 2 proposes a new fault location method based on sparse wide area measurements. One distinguishing feature of this method is its applicability to both transposed and untransposed transmission lines. In addition, the method is developed based on sparse-wide area measurement that may be taken far away from the faulted line. Shunt capacitances of transmission lines are also fully considered by the algorithm. Moreover, when synchronized measurements from multiple buses are available, an optimal estimator can be used to make the most use of measurements, and to detect and identify potential bad measurements.

Most of the existing fault location literatures discuss common shunt faults, including single line-to-ground faults, line-to-line faults, line-to-line-to-ground faults, and three-phase faults. However, in addition to common shunt faults, some complex faults may also occur in power systems. Among these complex faults, evolving fault and inter-circuit fault are two typical examples. Chapter 3 extends the method developed in Chapter 2 to deal with evolving faults. The proposed

wide-area fault location methods are immune to fault type evolution, and are applicable to both transposed and untransposed lines.

Chapter 4 discusses location of inter-circuit faults. Inter-circuit fault is a type of simultaneous fault, and it is the most common simultaneous fault type. Inter-circuit faults between each circuit in a double-circuit line is the most common inter-circuit fault. A fault location method for inter-circuit faults on double-circuit lines are developed and evaluated in Chapter 4.

Chapter 5 puts forward a fault location algorithm, which does not require line parameters information, for series-compensated transmission lines. Two-end synchronized voltage and current measurements are utilized. The proposed method is independent of source impedance and fully considers shunt capacitances of transmission lines.

KEYWORDS: fault location, untransposed lines, wide-area measurements, complex fault, parameter-free.

Xiangqing Jiao

April 21, 2017

FAULT LOCATION IN TRANSMISSION SYSTEMS USING SYNCHRONIZED MEASUREMENTS

By

Xiangqing Jiao

Dr. Yuan Liao

Director of Dissertation

Dr. Caicheng Lu

Director of Graduate

April 21, 2017

Date

Dedicated to my family and my motherland

ACKNOWLEDGEMENTS

I would like to express my deepest gratitude to my advisor, Dr. Yuan Liao, who has guided me with his exceptional intelligence and generosity. He is not only an uncommonly nice and intelligent advisor, but also my role model. I would also like to express my great appreciation to my committee members, Dr. Paul Dolloff, Dr. Yuming Zhang, and Dr. Zongming Fei for their invaluable advices, insightful comments, and encouragement. In addition, a thank you to Dr. Joseph Sottile for his willingness to serve as the outside examiner of my defense.

My sincere thanks also go to my friends Wanjing Xiu, Guangbin Zhang, Aleksi Paaso, Yukang Liu, Jiaxiong Chen and Ke Xu. I also want to thank Dr. Feng Gao and Dr. Hongtao Wang for their endless support.

Finally, I would like to thank my family for their unconditional love, and wish everyone good health.

TABLE OF CONTENTS

List of Tables

List of Figures

Chapter 1 Introduction

1.1 Background

Electric power system is one of the greatest engineering achievements in the last century. Electricity is generated at generating sites, and delivered to the end consumers remarkably far away. Transmission network plays a significant role in such bulk movement of electric energy. Modern transmission systems span over vast geographic area, and occasionally suffer from short-circuit faults. Faults are generally caused by random and unpredictable events such as falling of tree branches, lightning, wind, car accident, storm, etc. A fault usually results in a large amount of current flow that will lead to equipment damage, and even severe large area outages. Once a fault occurs in transmission networks, it is pivotal for utility engineers to repair the faulted line and restore power as soon as possible. Therefore, accurate and fast transmission line fault location plays a critical role in quick power system restoration.

In the past, numerous algorithms have been developed to pinpoint the locations of faults in transmission systems [3]-[26]. Most of the existing methods require measurements from at least one end of the faulted line. To omit the necessity of local requirements, this dissertation develops new fault location

methods based on sparse wide-area measurements that may be taken far away from the faulted line. Wide-area measurements are captured by phasor measurement units (PMUs). IEEE standard C37.118.1-2011 defines PMU as a device that produces synchronized phasor, frequency and rate of change of frequency estimates from voltage and/or current signals and a time synchronization signal [27]. According to the standard C37.118.1-2011, the required reporting rates of PMU should either be 10, 25, or 50 frames per second for a 50 Hz system, and it may be 10, 12, 15, 20, 30, 60 frames per second for a 60 Hz system [27]. Compared with conventional measurements from supervisory control and data acquisition (SCADA) system, PMU is able to provide direct and time-synchronized phasor measurements at a higher sampling frequency. The voltage and current phasors are measured with respect to a reference signal over the global positioning satellite (GPS) system, and thus are synchronized. Hence, PMUs installed at different locations in a transmission system can provide measurements that correspond to the same event.

A variety of power system applications benefit from the increasing deployment of PMUs in power systems in the last decades. The work reported in this dissertation is primarily focused on using synchrophasors to realize wide-area fault location in transmission systems. Also, since transmission line parameters are

critical inputs for the proposed fault location methods, estimation of line parameters along with fault locations based on synchrophasors is discussed.

1.2. Review of Fault Location Methods

Transmission systems are subject to many types of fault. The principal types of fault include:

a. single line-to-ground fault, which is denoted as LG fault;

b. line-to-line fault, which is denoted as LL fault,

c. double-line-to-ground fault, which is denoted as LLG fault,

d. three-phase fault, which is denoted as LLL fault,

e. three-phase-to-ground fault, which is denoted as LLLG fault.

These types of faults are known as common shunt faults or common short-circuit faults [1]. In balanced transmission lines, all of the faults listed above except the three-phase short-circuit with or without earth connection cause imbalance between phases, and are called unsymmetrical faults.

In addition to these principal fault types, other kinds of fault may also occur, and these faults could be more complicated. Faults sometimes occur simultaneously at separate locations in a system, or change from one type to another over time. A fault may also occur between two transmission lines running in parallel, e.g. between two lines in a double-circuit transmission structure. These

types of faults are known as complex fault [2], and are less studied in the existing literatures.

A considerable number of studies have been done on fault location in transmission lines [3]-[26]. These location approaches can be broadly classified into two categories: impedance based location methods and travelling-wave based location methods. Impedance based methods can be further divided into phasor based methods and time-domain based methods. Alternatively, depending on the source of measurements, conventional impedance-based fault location methods can be divided into single-end methods and double-end methods. Single-end impedance based methods utilize voltage and/or current measurements at only one end of the faulted line; while double-end impedance based method use synchronized or unsynchronized measurements from both ends.

A review of impedance based fault location methods are presented as follows: In 1979, the authors of [3] developed an online digital fault locator which calculated fault distance based on measurement on the ratio of reactance of the line from the device to fault point. In 1988, M.S. Sachdev and R. Agarwal proposed a method that used the post fault voltage and current from two end terminals to pinpoint fault location [4]. The authors of [5] also utilize measurements from both ends of the studied transmission line to calculate fault distance, and the measurements do not have to be synchronized. Similarly, the author of [6]

proposed a method for multi-terminal single transmission lines using asynchronous samples from each terminal. In 1991, the authors of [7] proposed a fault location technique for multi-terminal two parallel transmission lines. M. Kezunovic *et al*. propose a fault location method that utilizes digital fault recorders equipped with Global Positioning System (GPS) to retrieve synchronized data from two end terminals [8]. The fault location technique proposed in [9] uses PMU at both ends of a transmission line to get synchronized voltage and current data. The author of [10] proposes several algorithms utilizing only voltage measurements, which omits possible errors caused by saturation of current transformers. The authors of [11] design an algorithm that pinpoints the fault by comparing the recorded voltage sag pattern to the patterns obtained in simulation by placing faults at different buses. In [12], fault location on a single multi-terminal line is identified iteratively by using synchronized voltage and current measurements from all terminals. A time-domain fault location algorithm for HVDC transmission lines is proposed in [14]. The proposed method incorporates the traveling-wave theory with the Bergeron time-domain method, and does not require synchronization of measurements. Reference [15] proposes a double-circuit line fault location algorithm based on modifying the apparent impedance using modal transformation. The authors of [16] employ single-ended measurements to locate faults, as well as to determine fault types and phases.

Wang et al. couple the impedance fault location method and traveling-wave method to pinpoint faults [17]. Fault locations may also be identified based on wide area measurements. The authors of [18] uses gradient descent method to identify faulted zone and fault locations. In [19], detection of faults is achieved based on PMU measurements obtained from a single generator bus, and the fault locations can be determined based on analysis of variations of equivalent voltage phasor angle at any one of the generator buses. The authors of [20] constructed system equations around the parallel loops of sequence networks to solve the fault location for a double-circuit line.

Some traveling-wave based fault location methods are reviewed as follows: Fault location on transmission lines using traveling-wave was first proposed by Röhrig in 1931 [21]. When a fault occurs on a transmission line, an electrical pulse originating from the fault point propagates along the transmission line away from the fault point. The time of pulse return indicates the distance to the fault point. One disadvantage of the traveling-wave method is that wave propagation can be significantly affected by system parameters and network configuration [22]. It is also quite challenging to locate faults close to a bus or faults with near zero inception angle [23]. In [24], a double end traveling-wave based fault location method is proposed. In [25], a traveling-wave fault location method that does not require time synchronization and wave polarity identification is developed. The

method developed in [26] estimates the Lipschitz exponent of the second transient wave-front signal, and uses it to determine the frequency component of the traveling-wave and the fault location.

1.3 Motivation and Objectives

As discussed above, conventional fault location methods require local measurements from at least one end of the faulted line. Such methods will fail to locate faults when monitoring devices at either end of the faulted line fails to take qualified measurements, or when monitoring devices are not available at either end of the faulted line. Methods were proposed using sparse measurements for fault location [28]. However, the methods assume transposed lines.

As a matter of fact, most of the existing studies share an assumption that transmission lines are fully transposed. However, in practice, untransposed lines are widely used in modern power systems. Unlike transposed lines, untransposed line introduces imbalance into transmission systems, and some fault location methods may be no longer applicable in such condition [29].

Moreover, traditional fault location algorithms assume fault conditions are stationary. However, not all fault conditions remain unchanged over the fault period. Evolving faults are types of faults such that the faulted phases change over time. Other complex fault types, such as inter-circuit faults, are usually neglected by conventional methods.

To complement these gaps, this dissertation aims to use wide-area measurements to pinpoint faults in transmission lines. The desired features of the proposed method should include:

a. ability to locate faults precisely;
b. ability to deal with both transposed and untransposed transmission lines;
c. ability to locate faults with only sparse wide-area measurements;
d. ability to deal with some complex faults
e. ability to fully consider shunt capacitances of transmission lines

1.4 Dissertation Outline

In this dissertation, Chapter 2 is dedicated to wide-area fault location algorithm for untransposed/transposed transmission lines. First, the fault location approach based on single bus measurement is presented. Then, a two-bus fault location algorithm is discussed. When measurements from multiple buses are available, an optimal estimator is designed and used to estimate fault locations as well as to detect/identify possible bad measurements.

Chapter 3 and Chapter 4 focus on complex faults, including evolving fault, and inter-circuit fault. In the beginning of Chapter 3 and Chapter 4, the backgrounds of the studied complex faults are reviewed. The rest of these two chapters extends the method developed in Chapter 2, and adapts it to deal with

complex faults. Evaluation studies based on Electromagnetic Transient Program (EMTP) is carried out, and verifies the effectiveness and accuracy of the proposed methods.

The fault location methods developed in Chapter 1 – Chapter 4 are based on wide-area measurements, and requires system information such as line parameters. As supplementary work to the previous chapters, Chapter 5 develops a fault location method that does not require line parameters information. The proposed method deals with series-compensated transmission lines, and is based on two-end voltage and current measurements. Line parameters, along with fault locations, can be estimated online. The information of the series compensator is not a prerequisite either.

Finally, a conclusion on the entire presented fault location work is made in Chapter 6.

Chapter 2 Fault Location for Untransposed/Transposed Transmission Lines Using Sparse Wide Area Measurements

2.1 Introduction

Compared with conventional fault location methods, wide-area methods can determine the locations of faults in the entire transmission network, using only a limited amount of synchrophasors. In the last decade, some wide-area fault location methods have been put forward. In [30], a traveling-wave based wide-area fault location method is proposed. The method requires several synchronized measurements of transient voltages from strategically distributed monitoring devices. Fault locations are derived by extracting the arrival time of voltage traveling-waves at different monitoring devices. The authors of [28] propose a method to locate faults on a double-circuit transmission line by using sparse voltage measurements. Fault type information is required by this algorithm, and the line is assumed to be transposed. In [31], based on the positive-sequence network, suspicious fault regions and fault locations can be determined. Wide area measurements have been adopted to in power system protection as well. Reference [32] presents a remote backup protection scheme to detect faults using synchrophasors, but without calculation of the fault location. The author of [33]

and [34] puts forward distribution system fault location method based on measurements from substation.

Most of the existing studies on transmission line fault location only consider transposed lines. The positions of a transposed line's conductors are exchanged at regular intervals along the line. Such transposition results in equal average inductance and shunt capacitance for each conductor over the whole transposition cycle [29].

However, in some cases, untransposed transmission lines are preferred over transposed lines, due to technical and economic factors such as additional cost of transposition tower, corridor limitation, reliability of transposition tower structure, etc. [35]-[38] In practice, most of the EHV/UHV transmission lines are untransposed [39]. In the context of untransposed lines, the fault location methods based on symmetrical component theory are no longer applicable.

To deal with untransposed lines, this chapter presents a general fault location method that is applicable to both transposed and untransposed lines. The method is developed based on sparse wide-area voltage phasor measurement, and fully considers the shunt capacitances of transmission lines, by using distributed parameter line model. The method is applicable to any principal types of faults, and does not demand fault classification. Therefore, the potential error due to fault type misidentification is eliminated. Moreover, the proposed method is applicable

to both single-circuit and double-circuit transmission lines. Finally, when redundant measurements are available, an optimal estimator can be used to make the most of multiple measurements, and to identify/detect potential bad measurements. Note that the fault types in this chapter refers to the principal fault types (LG, LL, LLG, LLL, and LLLG faults). A practical assumption of the proposed algorithm is that the network's parameter and topology are known.

In the rest of this chapter, Section 2.2 introduces the proposed wide-area fault location method based on voltage measurements from a single bus. The proposed method can accurately locate faults on both single-circuit and double-circuit transmission lines. When measurements from two buses are available, a two-bus fault location algorithm can be used. An optimal estimator is designed in Section 2.3, based on which potential bad measurements can be detected and identified. Evaluation studies under a variety of fault conditions are exhibited in Section 2.4, followed by the summary.

2.2 Fault Location Algorithm for Untransposed/Transposed Transmission Lines Based on Sparse Wide-Area Measurements

The proposed method is based on the bus impedance matrix concept and is described as follows: In the during-fault network, a fictitious bus is added at the assumed fault point. Then, the transfer impedances between the fictitious bus and any other buses, along with the driving point impedances at the fictitious bus, can be expressed as functions of the unknown fault distance. Transfer impedances refer to the off-diagonal elements in the bus impedance matrix, and driving point impedances refer to the diagonal elements in the bus impedance matrix [29]. Based on the short-circuit analysis, the voltage, current and power at the fault bus can be derived in terms of the given voltage measurements at a certain bus, the corresponding transfer impedance, and driving point impedance. Consequently, they can be revealed as functions of the fault location. Since the fault resistance only consume real power, the reactive power consumed will be zero, based on which the fault location can be determined.

The method is developed in phase domain to accommodate the inherent unbalances of the untransposed transmission lines.

2.2.1 Derivation of Transfer and Driving Point Impedances

Assume a fault occurs on a single-circuit untransposed line as depicted in Figure 2.1 (the remaining part of the transmission system is not shown). The following notations are adopted in this chapter:

n total number of nodes of the entire transmission system without counting fault nodes;

$\boldsymbol{Z}_0$ bus impedance matrix of the pre-fault network, excluding the fictitious fault nodes; the size of $\boldsymbol{Z}_0$ is n by n, since n nodes are included in the pre-fault network;

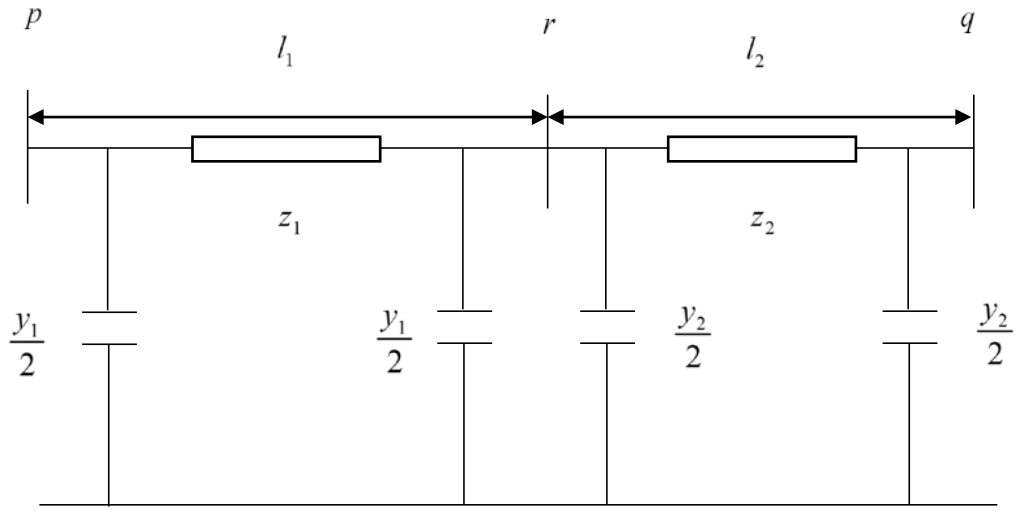

Figure 2.1 Single-circuit untransposed line section of a transmission system.

$\boldsymbol{Z}$	bus impedance matrix of the during-fault network; the size of $\boldsymbol{Z}$ is (n+3) by (n+3); the element on the kth row and jth column is denoted as Z_{kj};
p, q	buses of the two ends of the studied line section;
$p_1, p_2, p_3, q_1, q_2, q_3$	nodes of the two ends of the studied line section;
r	fictitious bus added at the assumed fault point;
r_1, r_2, r_3	fictitious nodes added at the assumed fault location;
$\boldsymbol{E_p}, \boldsymbol{E_q}$	node voltage vectors at bus p and bus q, respectively, where $\boldsymbol{E_p} = [E_{p_1}, E_{p_2}, E_{p_3}]^T$ and $\boldsymbol{E_q} = [E_{q_1}, E_{q_2}, E_{q_3}]^T$, and $[.]^T$ represents transpose of its argument;
$\boldsymbol{E_r}$	node voltage vector at the fictitious bus, bus r, where $\boldsymbol{E_r} = [E_{r_1}, E_{r_2}, E_{r_3}]^T$;
l_1	length of the line between bus p and bus q;
l_2	length of the line between bus p and bus q;
$\boldsymbol{x}, \boldsymbol{y}$	per unit length impedance and admittance matrix of the studied line section.

The during-fault bus impedance matrix $\boldsymbol{Z}$ shares the same first n rows and first n columns with $\boldsymbol{Z}_0$. The other rows and columns of $\boldsymbol{Z}$ consist of transfer and

driving point impedances related to the fault nodes. The following part of this section illustrates the derivation of these impedances.

The equivalent PI circuit parameters for each segment of the untransposed line can be expressed as follows [40]:

$$\boldsymbol{z}_i = \boldsymbol{zB}diag[\sinh(\boldsymbol{\gamma} l_i)./\boldsymbol{\gamma}]\boldsymbol{B}^{-1}, \qquad i = 1,2 \tag{2.1}$$

$$\frac{\boldsymbol{y}_i}{2} = \boldsymbol{B}diag[\tanh(\boldsymbol{\gamma} l_i/2)./\boldsymbol{\gamma}]\boldsymbol{B}^{-1}\boldsymbol{y}, \quad i = 1,2 \tag{2.2}$$

where $diag\{\cdot\}$ returns a square diagonal matrix with the elements of input vector on the its diagonal; $\boldsymbol{B}$ is the eigenvector of $\boldsymbol{yz}$; './' for element-wise division; $\boldsymbol{\gamma}$ is a vector composed of γ_j, the square root of the *j*th eigenvalue of $\boldsymbol{yz}$, $j = 1,2,3$ for single-circuit lines, and $j = 1,2,...,6$ for double-circuit lines.

Assume *k* is an arbitrary bus in the system except the fictitious bus, and bus *k* consists of nodes k_1, k_2, and k_3. Based on the definition of transfer impedance, the value of the transfer impedance between the node k_i, $i = 1,2,3$, and a fault node will be equal to the voltage at the fault node, when all the sources in the network are removed and a current of 1 A is injected into the node k_i.

By removing all the sources in the network, injecting 1 A current into node k_i, and apply the Kirchhoff's Current Law (KCL) at bus *r* gives

$$\frac{\boldsymbol{y}_1}{2}\boldsymbol{E}_r + \frac{\boldsymbol{y}_2}{2}\boldsymbol{E}_r + \boldsymbol{z}_1^{-1}(\boldsymbol{E}_r - \boldsymbol{E}_p) + \boldsymbol{z}_2^{-1}(\boldsymbol{E}_r - \boldsymbol{E}_q) = 0 \tag{2.3}$$

Therefore, the node voltage vector at the fictitious bus, $\boldsymbol{E}_r$, is calculated as

$$\boldsymbol{E}_r = (\frac{\boldsymbol{y}_1}{2} + \frac{\boldsymbol{y}_2}{2} + \boldsymbol{z}_1^{-1} + \boldsymbol{z}_2^{-1})^{-1}(\boldsymbol{z}_1^{-1}\boldsymbol{E}_p + \boldsymbol{z}_2^{-1}\boldsymbol{E}_q) \tag{2.4}$$

Then, the transfer impedances between the node k_i and the fault node can be expressed as

$$\boldsymbol{Z}_{\boldsymbol{k_i r}} = (\frac{\boldsymbol{y}_1}{2} + \frac{\boldsymbol{y}_2}{2} + \boldsymbol{z}_1^{-1} + \boldsymbol{z}_2^{-1})^{-1}(\boldsymbol{z}_1^{-1}\boldsymbol{Z}_{\boldsymbol{k_i p}} + \boldsymbol{z}_2^{-1}\boldsymbol{Z}_{\boldsymbol{k_i q}}), \quad i = 1,2,3 \tag{2.5}$$

where,

$$\boldsymbol{Z}_{\boldsymbol{k_i r}} = [Z_{k_i r_1}, Z_{k_i r_2}, Z_{k_i r_3}]^T \tag{2.6}$$

$$\boldsymbol{Z}_{\boldsymbol{k_i p}} = [Z_{k_i p_1}, Z_{k_i p_2}, Z_{k_i p_3}]^T \tag{2.7}$$

$$\boldsymbol{Z}_{\boldsymbol{k_i q}} = [Z_{k_i q_1}, Z_{k_i q_2}, Z_{k_i q_3}]^T \tag{2.8}$$

The transfer impedances $Z_{k_i p_1}$, $Z_{k_i q_1}$ etc. are constant elements in the pre-fault bus impedance matrix $\boldsymbol{Z}_0$. Therefore, the transfer impedances between the non-fault node k_i and the fault nodes are functions of the fault distance l_1.

Similarly, by removing all sources in the network, injecting 1 A current into the fault node r_i (i = 1, 2, 3), and applying KCL at bus r, the driving point impedances and transfer impedances related to the fault nodes are derived as

$$\boldsymbol{Z}_{rr_i} = (\frac{\boldsymbol{y}_1}{2} + \frac{\boldsymbol{y}_2}{2} + \boldsymbol{z}_1^{-1} + \boldsymbol{z}_2^{-1})^{-1}(\boldsymbol{z}_1^{-1}\boldsymbol{Z}_{pr_i} + \boldsymbol{z}_2^{-1}\boldsymbol{Z}_{qr_i} + \boldsymbol{u}_i), \qquad i = 1,2,3 \tag{2.9}$$

where $\boldsymbol{u}$ is a three by three identity matrix, whose ith column is denoted by $\boldsymbol{u}_i$; $\boldsymbol{Z}_{pr_i}$ consists of transfer impedances between nodes on bus p and the fault node r_i, and $\boldsymbol{Z}_{qr_i}$ consists of transfer impedances between nodes bus q and the fault node r_i. It notes that $\boldsymbol{u}_i$ corresponds to the current injection into the ith node of the faulted bus.

Therefore, the transfer impedances between the fault nodes, and the driving point impedances at fault nodes are derived as functions of the unknown fault distance l_1.

2.2.2 Derivation of Voltage at Fault Nodes and Fault Current during the Fault Period

Using the driving point impedances and transfer impedances derived above, the voltage at the fault nodes and the fault current during that fault can be determined.

Assume that the arbitrary bus k consists of nodes k_1, k_2 and k_3. The voltage change due to the fault, *i.e.* the superimposed voltage at bus k, $\boldsymbol{\Delta E_k}$, can be written as

$$\boldsymbol{\Delta E_k} = [\Delta E_{k_1}, \Delta E_{k_2}, \Delta E_{k_3}]^T \tag{2.10}$$

Based on the superimposed theory, the superimposed voltage during a fault can be obtained as:

$$\boldsymbol{\Delta E_k} = -\boldsymbol{Z_{kr}} \boldsymbol{I_f} \tag{2.11}$$

where $\boldsymbol{Z_{kr}}$ consists of the transfer impedances between the nodes at bus k and the faulted nodes, and $\boldsymbol{I_f}$ is the fault current.

Subsequently, the fault current can be expressed in terms of measurements $\boldsymbol{\Delta E_k}$ as

$$\boldsymbol{I_f} = -(\boldsymbol{Z_{kr}}^T \boldsymbol{Z_{kr}})^{-1} (\boldsymbol{Z_{kr}}^T \boldsymbol{\Delta E_k}) \tag{2.12}$$

The pre-fault voltages at the fault nodes can be expressed in terms of the fault location as

$$\boldsymbol{E_{r0}} = (\frac{\boldsymbol{y_1}}{2} + \frac{\boldsymbol{y_2}}{2} + \boldsymbol{z_1}^{-1} + \boldsymbol{z_2}^{-1})^{-1} (\boldsymbol{z_1}^{-1} \boldsymbol{E_{p0}} + \boldsymbol{z_2}^{-1} \boldsymbol{E_{q0}}) \tag{2.13}$$

where $\boldsymbol{E}_{p0}$ and $\boldsymbol{E}_{q0}$ are the pre-fault node voltage vectors at bus p ans bus q, respectively. These pre-fault voltages can be estimated based on the pre-fault network conditions.

The during-fault voltages at the fault nodes can be expressed as

$$\boldsymbol{E}_r = \boldsymbol{E}_{r0} - \boldsymbol{Z}_{rr}\boldsymbol{I}_f \tag{2.14}$$

Equations (2.12) and (2.14) represent the fault current and the voltages at the faulted nodes in terms of the transfer and driving point impedances, and consequently in terms of the unknown fault location.

2.2.3 Location of Faults Based on Single-Bus Measurements

The complex power consumed by the fault resistance is the product of fault voltage and conjugate of fault current, and is obtained as:

$$S = -\boldsymbol{E}_r^{\,T}[(\boldsymbol{Z}_{kr}^{\,T}\boldsymbol{Z}_{kr})^{-1}(\boldsymbol{Z}_{kr}^{\,T}\boldsymbol{\Delta E}_k)]^* \tag{2.15}$$

where, the asterisk sign denotes complex conjugate of its argument. A practical assumption is that the fault is pure resistive. Since the fault resistances only consumes real power, so the imaginary part of S is zero:

$$\text{Imag}(S) = 0 \tag{2.16}$$

It can be observed that (2.16) only has one unknown variable l_1 that is the distance from the bus p to the fault point r. The fault location can consequently be determined by the Newton-Raphson technique. The Newton-Raphson approach is described as follows:

$$m_{v+1} = m_v + \Delta m_v \tag{2.17}$$

$$\Delta m_v = -H_v Q(m_v) \tag{2.18}$$

$$H_v = \frac{\partial Q(m)}{\partial m}|_{m=m_V} \tag{2.19}$$

where the following notations are used:

m_v	fault distance variable at the vth iteration;
m_{v+1}	fault distance variable after the vth iteration;
Δm_v	fault distance variable update at the vth iteration;
H_v	Jacobian matrix when $m = m_v$;
$Q(m_v)$	imaginary power function when $m = m_v$;
v	iteration number starting from 0.

When the variable update reaches within the specified tolerance, the iterative process can be terminated. Educated initial value for variable should be

provided, which in this case is 0.5. The Jacobian matrix can be obtained based on numerical method, in order to obviate the need to derive the complicated analytical form of the derivatives of Jacobian matrix and to still maintain high accuracy of fault location estimate.

It should be noted that the fault type information is not used in the above derivation, and neither is the fault resistance. It is also noted that this method is certainly applicable to transposed lines as well.

Also, the system loading conditions do not affect the accuracy of fault location. The core equation to determine the fault location is (2.15). In (2.15), the accuracy of computation or measurement of variables on the right-hand-side are not affected by loading condition. Thus, the location accuracy is not affected by loading condition.

2.2.4 Cases When the Faulted Line is A Double-Circuit Line

When the faulted line is a double-circuit line, a fictitious bus containing six nodes are added to the assumed fault location in the network.

The equivalent Pi circuit line parameters can be calculated following the equations (2.1)-(2.2). It is noted that, in the case of double-circuit lines, $\boldsymbol{z}_1, \boldsymbol{y}_1, \boldsymbol{z}_2, \boldsymbol{y}_2$ are six by six matrices. The transfer impedances between the nodes of the bus k and the faulted nodes can be derived as

$$\boldsymbol{Z}_{k_i r} = (\frac{\boldsymbol{y}_1}{2} + \frac{\boldsymbol{y}_2}{2} + \boldsymbol{z}_1^{-1} + \boldsymbol{z}_2^{-1})^{-1}(\boldsymbol{z}_1^{-1}[\boldsymbol{Z}_{k_i p}, \boldsymbol{Z}_{k_i p}]^T + \boldsymbol{z}_2^{-1}[\boldsymbol{Z}_{k_i q}, \boldsymbol{Z}_{k_i q}]^T), \quad i = 1,2,\ldots,6 \quad (2.20)$$

The transfer impedances and the driving point impedances related to the faulted nodes are expressed as

$$\boldsymbol{Z}_{rr_i} = (\frac{\boldsymbol{y}_1}{2} + \frac{\boldsymbol{y}_2}{2} + \boldsymbol{z}_1^{-1} + \boldsymbol{z}_2^{-1})^{-1}(\boldsymbol{z}_1^{-1}[\boldsymbol{Z}_{pr_i}, \boldsymbol{Z}_{pr_i}]^T + \boldsymbol{z}_2^{-1}[\boldsymbol{Z}_{qr_i}, \boldsymbol{Z}_{qr_i}]^T + \boldsymbol{g}_i), \quad i = 1,2,\ldots,6 \quad (2.21)$$

where $\boldsymbol{Z}_{pr_i}$ and $\boldsymbol{Z}_{qr_i}$ can be calculated based on (2.20), and $\boldsymbol{g}$ is a six by six identify matrix whose *i*th column is denoted by $\boldsymbol{g}_i$.

The pre-fault voltage at the fictitious bus is

$$\boldsymbol{E}_{r0} = (\frac{\boldsymbol{y}_1}{2} + \frac{\boldsymbol{y}_2}{2} + \boldsymbol{z}_1^{-1} + \boldsymbol{z}_2^{-1})^{-1}(\boldsymbol{z}_1^{-1}[\boldsymbol{E}_{p0}, \boldsymbol{E}_{p0}]^T + \boldsymbol{z}_2^{-1}[\boldsymbol{E}_{q0}, \boldsymbol{E}_{q0}]^T) \quad (2.22)$$

The during-fault voltage the fictitious bus and the fault current can be calculated based on (2.14) and (2.12). The fault location can then be solved based on (2.16).

2.2.5 Cases When Measurements from Two Buses Are Available

For the scenarios where measurements from two buses are available, a two-bus algorithm is developed based on synchronized measurements. Suppose voltage measurements are available from non-fault buses *k* and *k*'

($k, k' = 1,2,...,n$), and the two buses' measurements are synchronized. For bus k', similar to (2.11), the following equation exists:

$$\boldsymbol{\Delta E}_{k'} = -\boldsymbol{Z}_{k'r}\boldsymbol{I}_f \tag{2.23}$$

Eliminating $\boldsymbol{I}_f$ from (2.11) and (2.23) results in

$$(\boldsymbol{Z}_{k'r}{}^T\boldsymbol{Z}_{k'r})^{-1}(\boldsymbol{Z}_{k'r}{}^T\boldsymbol{\Delta E}_{k'}) - (\boldsymbol{Z}_{kr}{}^T\boldsymbol{Z}_{kr})^{-1}(\boldsymbol{Z}_{kr}{}^T\boldsymbol{\Delta E}_k) = 0 \tag{2.24}$$

Equation (2.24) only includes one unknown variable, the fault distance. Three equations will be yielded from (2.24) for phase A, B, and C, respectively, which can then be separated into six real equation. Subsequently, the fault location can be solved based on this equation.

If the measurements from buses k and k' are not synchronized, by equaling the magnitudes of the fault current derived based on the two sets of measurements, the fault location can still be obtained.

When the two buses' measurements are not synchronized, the fault current calculated based on measurements from bus k is $-(\boldsymbol{Z}_{kr}^T\boldsymbol{Z}_{kr})^{-1}(\boldsymbol{Z}_{kr}^T\boldsymbol{\Delta E}_k)$, while the current value based on the measurements from bus k' is $(\boldsymbol{Z}_{k'r}{}^T\boldsymbol{Z}_{k'r})^{-1}(\boldsymbol{Z}_{k'r}{}^T\boldsymbol{\Delta E}_{k'}e^{j\delta})$, where δ represents the unsyncrhonization angle. Equaling the magnitudes of these two fault currents yields

$$|(\boldsymbol{Z}_{k'r}{}^T\boldsymbol{Z}_{k'r})^{-1}(\boldsymbol{Z}_{k'r}{}^T\boldsymbol{\Delta E}_{k'})| - |(\boldsymbol{Z}_{kr}{}^T\boldsymbol{Z}_{kr})^{-1}(\boldsymbol{Z}_{kr}{}^T\boldsymbol{\Delta E}_k)| = 0 \tag{2.25}$$

where |.| returns the magnitude of its argument. Following a similar process described in (2.17)-(2.19), the fault location can be derived.

2.3 Optimal Estimation of Fault Locations Considering Possible Measurement Errors

In this section, an optimal fault location estimator is developed, which can detect and identify possible measurement errors when synchronized measurements are available at multiple buses in the system.

2.3.1 Proposed Optimal Estimator for Fault Locations

Suppose synchronized superimposed voltage measurements at buses $n_1, n_2, ..., n_N$ are available, which forms the following vector:

$$\boldsymbol{M} = [\Delta E_{n_{1a}}, \Delta E_{n_{1b}}, \Delta E_{n_{1c}}, \Delta E_{n_{2a}}, \Delta E_{n_{2b}}, \Delta E_{n_{2c}}, \Delta E_{n_{Na}}, \Delta E_{n_{Nb}}, \Delta E_{n_{Nc}}]^T \quad (2.26)$$

where N is the total number of recordable buses, $\Delta E_{n_{ia}}$, $\Delta E_{n_{ib}}$ and $\Delta E_{n_{ic}}$ are the phase A, B, C superimposed voltages at the bus n_i ($i = 1, \ldots, N$).

Defining the unknown variable as

$$\boldsymbol{X} = [x_1, x_2, ..., x_{6N}, x_{6N+1}] \quad (2.27)$$

where x_{2i-1}, x_{2i}, $i = 1,...,3N$ are the variables required to represent the complex superimposed node voltages caused by the fault (i.e. the *i*th superimposed voltage

equals $x_{2i-1}e^{jx_{2i}}$, where j denotes the imaginary unit here), and x_{6N+1} is the unknown fault distance variable.

The total number of combination of two buses out of the measurable buses is $W = C_N^2$, where C represents the combination calculation. One single such combination will yield six real equations. In total, we can have $6W$ such equations, and each of them is denoted as $f_i(\boldsymbol{X})$. Then the function vector $\boldsymbol{F(X)}$ is defined as

$$\boldsymbol{F}_i(\boldsymbol{X}) = f_i(\boldsymbol{X}) \qquad i = 1,\ldots,6W \tag{2.28}$$

$$\boldsymbol{F}_{6W+2i-1}(\boldsymbol{X}) = \mathrm{Re}(x_{2i-1}e^{jx_{2i}}) \qquad i = 1,...,3N \tag{2.29}$$

$$\boldsymbol{F}_{6W+2i}(\boldsymbol{X}) = \mathrm{Im}(x_{2i-1}e^{jx_{2i}}) \qquad i = 1,...,3N \tag{2.30}$$

It can be observed that $\boldsymbol{F(X)}$ has $6W + 6N$ elements.

Define $\boldsymbol{Y}$ as the measurement vector, which is formed as

$$\boldsymbol{Y}_i = 0, \qquad i = 1,...,6W \tag{2.31}$$

$$\boldsymbol{Y}_{6W+2i-1} = \mathrm{Re}(M_i), \qquad i = 1,...,3N \tag{2.32}$$

$$\boldsymbol{Y}_{6W+2i} = \mathrm{Im}(M_i), \qquad i = 1,...,3N \tag{2.33}$$

The relationship between the measurement vector and function vector is

$$\boldsymbol{Y} = \boldsymbol{F(X)} + \boldsymbol{\mu} \tag{2.34}$$

where $\boldsymbol{\mu}$ is a vector representing measurement errors which are dependent on meter accuracy. The more accurate a meter is, the less the corresponding element in $\boldsymbol{\mu}$ is.

The vector of measurement errors is defined as the difference between the measurement vector and the function vector as

$$\boldsymbol{\mu} = \boldsymbol{Y} - \boldsymbol{F}(\boldsymbol{X}) \tag{2.35}$$

By minimizing the following cost function, the optimal estimate of $\boldsymbol{X}$ can be obtained.

$$J = [\boldsymbol{Y} - \boldsymbol{F(X)}]^T \boldsymbol{R}^{-1} [\boldsymbol{Y} - \boldsymbol{F(X)}] \tag{2.36}$$

where the covariance matrix $\boldsymbol{R}$ is defined as

$$\boldsymbol{R} = E(\boldsymbol{\mu}\boldsymbol{\mu}^T) = diag(\sigma_1^2, ..., \sigma_{6W+6N}^2) \tag{2.37}$$

Here, $E(.)$ stands for the expected value of its argument. σ_i^2 is the variance corresponding to the *i*th measurement, with a smaller value indicating a higher accuracy. Equation (2.36) can be solved iteratively [41]. The iteration calculation is terminated when the biggest element of the unknown variable update is smaller than the desired tolerance. The starting value of $\boldsymbol{X}$ is chosen as: 0.1 p.u. and $\frac{\pi}{4}$ for

the superimposed voltage's magnitude and angel, respectively; 0.5 p.u. for the fault location estimate.

2.3.2 Detection and Identification of Measurement Errors

Chi-Square test can be utilized to detect the presence of bad measurement [42]. First, the expected value of the cost function is calculated, which is equal to the number of measurements minus the number of variables. Then the estimated value of the cost function, C_J, is obtained as:

$$C_J = \sum_{i=1}^{N} \frac{\hat{\mu}_i^2}{\sigma_i^2} \tag{2.38}$$

where,

$\hat{\mu}_i^2$ estimated measurement error in the *i*th measurement;

σ_i^2 variance of the error in the *i*th measurement;

N total number of measurement.

The threshold value, $\chi^2_{h,\alpha}$, can be calculated based on the number of degrees of freedom h, confidence level α, and the chi-square distribution. If $C_J \geq \chi^2_{h,\alpha}$, then the presence of bad measurements is suspected with a probability of $(1-\alpha)$. If bad data is detected, the normalized error will be calculated, and the measurement corresponding to the largest normalized error will be identified as

the bad data. Otherwise, for cases where $C_J < \chi^2_{h,\alpha}$, the measurement sets are assumed to be free of bad data.

2.4 Evaluation Studies

This section presents the evaluation simulation studies for verifying the developed fault location algorithms. The Electromagnetic Transients Program (EMTP) has been utilized to generate fault data for faults of different fault types, locations, and fault resistances [40].

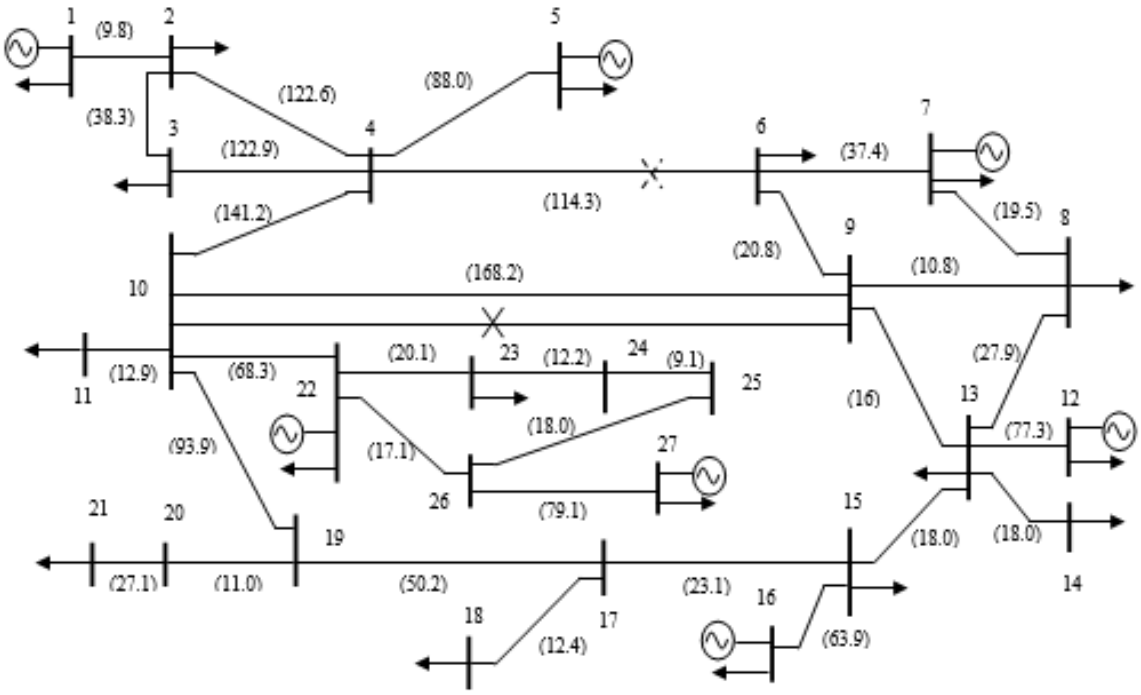

Figure 2.2 Diagram of the studied 27-bus transmission system

A 27-bus, 345-kV, 60-Hz transmission-line system is utilized for evaluation study, which is shown in Figure 2.2. The lengths of each line are labeled in miles in parenthesis. For single-circuit line fault location study, the fault is imposed on the section between bus 4 and bus 6, with the dashed cross denoting the fault point. For double-circuit line fault location study, the fault is assumed to fall on the section between bus 9 and bus 10, with the cross denoting the fault point. Both lines are untransposed lines and are modeled based on the distributed parameter line model in EMTP.

The developed algorithm has been implemented in Matlab. In the study, a starting value of 0.5 p.u. for the fault location is utilized, and all the cases except those where bad data exists converge within 10 iterations. The estimation accuracy is measured by the percentage error calculated as

$$\%\text{Error} = \frac{\left|\text{Actual Location - Estimated Location}\right|}{\text{Total Length of Faulted Line}} \times 100 \tag{2.39}$$

2.4.1 Fault Location Results for One-Bus and Two-Bus Algorithms

Table 2.1 and Table 2.2 present the fault location results on single-circuit untransposed lines. Different fault conditions with various fault types, resistances, and locations are studied.

The one-bus fault location results are listed in Table 2.1. In this table, columns 1-3 list the fault type, actual fault location, and fault resistance, respectively. The percentage errors of the estimation are listed in columns 4-6.

Fault location is measured from the beginning bus, i.e. bus 4 in this case, of the line section. Various fault resistances have been tested in the evaluation studies. It can be seen that accurate results are obtained even if measurements only from a single bus is available, which may not be necessarily from the terminal of the faulted line.

Table 2.2 presents representative fault location estimates using synchronized measurements from two buses obtained by the proposed method. The columns 1-3 provide the fault conditions, and the estimation results are listed in columns 4-7. It is observed that quite accurate results for fault location have been achieved by the developed algorithms.

Table 2.1 Fault Location Results for Single-Circuit Untransposed Lines Based on Measurements from One Bus

Fault type	Fault Loca. (p.u.)	Fault res. (Ω)	Est. error (%) using data from bus		
			3	11	21
AG	0.3	1	0.03	0.07	0.33
		5	0.03	0.09	0.60
		50	0.39	0.43	0.88
	0.8	1	0.22	0.30	0.90
		5	0.26	0.36	0.91
		50	0.31	0.43	0.89
BC	0.3	1	0.05	0.06	0.39
		10	0.09	0.11	0.43
		50	0.26	0.48	0.93
	0.7	1	0.13	0.10	0.04
		10	0.07	0.00	0.09
		50	0.20	0.44	0.31
BCG	0.3	1	0.03	0.01	0.28
		5	0.02	0.02	0.09
		50	0.02	0.02	0.67
	0.5	1	0.13	0.01	0.44
		5	0.12	0.04	0.32
		50	0.05	0.04	0.04
ABC	0.2	1	0.02	0.01	0.01
		5	0.03	0.03	0.05
		50	0.33	0.56	0.56
	0.7	1	0.03	0.02	0.02
		5	0.01	0.05	0.00
		50	0.60	0.67	0.46

Table 2.2 Fault Location Results for Single-Circuit Untransposed Lines Based on Measurements from Two Buses

Fault type	Fault Loca. (p.u.)	Fault res. (Ω)	Est. error (%) using data from buses			
			3&9	5&8	7&22	12&24
AG	0.3	1	0.09	0.06	0.07	0.17
		5	0.07	0.02	0.04	0.12
		50	0.09	0.07	0.26	0.17
	0.8	1	0.01	0.04	0.17	0.12
		5	0.01	0.02	0.20	0.19
		50	0.08	0.04	0.41	0.41
BC	0.3	1	0.01	0.03	0.16	0.16
		10	0.01	0.01	0.12	0.11
		50	0.01	0.02	0.22	0.23
	0.7	1	0.01	0.02	0.23	0.24
		10	0.01	0.01	0.19	0.19
		50	0.03	0.04	0.35	0.27
BCG	0.3	1	0.00	0.04	0.13	0.22
		5	0.00	0.04	0.14	0.22
		50	0.00	0.04	0.19	0.19
	0.5	1	0.02	0.01	0.15	0.12
		5	0.02	0.01	0.17	0.14
		50	0.01	0.03	0.22	0.21
ABC	0.2	1	0.02	0.02	0.03	0.11
		5	0.01	0.01	0.05	0.09
		50	0.00	0.01	0.33	0.21
	0.7	1	0.01	0.00	0.15	0.13
		5	0.00	0.00	0.16	0.11
		50	0.07	0.07	0.59	0.45

Table 2.3 and Table 2.4 exhibit the percentage fault location errors for double-circuit untransposed lines using measurement from a single bus and synchronized measurements from two buses, respectively. Various fault conditions have been tested in the simulation studies, and representative results are reported here. In Table 2.3 and Table 2.4, columns 1-3 are the fault type, actual fault location and fault resistance, respectively. The other columns are the fault location estimation errors based on measurements from different buses. It is seen that quite accurate estimates are produced by each algorithm.

When measurements from multiple buses are available, the developed optimal fault locator can be applied. Table 2.5 lists the optimal estimation results obtained by the developed method. To save space, the results for single- and double-circuit lines are presented in columns 4 and 5 of the same table, respectively. The single-circuit case uses measurements from buses 1, 5, 13 and 26, and the double-circuit case uses measurements from buses 3, 7, 13 and 21. It is evinced that the proposed method has yielded quite accurate results.

Table 2.3 Fault Location Results for Double-Circuit Untransposed Lines Based on Measurements from One Bus

Fault type	Fault Loca. (p.u.)	Fault res. (Ω)	Est. error (%) using data from bus		
			4	18	26
AG	0.3	1	0.15	0.18	0.23
		5	0.10	0.12	0.11
		50	0.20	0.22	0.04
	0.8	1	0.15	0.17	0.12
		5	0.03	0.09	0.03
		20	0.04	0.11	0.03
BC	0.3	1	0.10	0.06	0.18
		10	0.12	0.07	0.20
		20	0.14	0.09	0.22
	0.6	1	0.19	0.38	0.14
		10	0.22	0.50	0.15
		50	0.39	0.32	0.17
BCG	0.3	1	0.07	0.03	0.07
		5	0.08	0.03	0.17
		50	0.09	0.04	0.30
	0.7	1	0.05	0.05	0.07
		5	0.06	0.05	0.08
		50	0.08	0.07	0.10
ABC	0.2	1	0.01	0.02	0.08
		5	0.01	0.02	0.10
		50	0.04	0.00	0.41
	0.6	1	0.04	0.28	0.04
		5	0.04	0.28	0.04
		50	0.10	0.13	0.17

Table 2.4 Fault Location Results for Double-Circuit Untransposed Lines Based on Measurements from Two Buses

Fault type	Fault Loca. (p.u.)	Fault res. (Ω)	Est. error (%) using data from buses			
			4&8	6&11	13&22	17&26
AG	0.3	1	0.02	0.02	0.07	0.08
		5	0.05	0.04	0.10	0.11
		50	0.12	0.15	0.16	0.15
	0.8	1	0.01	0.03	0.06	0.10
		5	0.01	0.02	0.08	0.16
		20	0.03	0.05	0.15	0.26
BC	0.3	1	0.06	0.03	0.09	0.10
		10	0.08	0.03	0.10	0.12
		20	0.11	0.03	0.12	0.14
	0.5	1	0.05	0.04	0.09	0.10
		5	0.06	0.04	0.09	0.10
		20	0.10	0.03	0.11	0.14
BCG	0.3	1	0.01	0.03	0.06	0.07
		5	0.01	0.03	0.07	0.07
		50	0.03	0.03	0.08	0.09
	0.7	1	0.05	0.05	0.08	0.08
		5	0.05	0.05	0.08	0.09
		50	0.06	0.05	0.09	0.10
ABC	0.2	1	0.02	0.03	0.06	0.07
		5	0.05	0.03	0.08	0.09
		50	0.34	0.04	0.30	0.39
	0.6	1	0.06	0.07	0.09	0.10
		5	0.06	0.07	0.09	0.11
		50	0.26	0.02	0.23	0.34

Table 2.5 Optimal Fault Location Results for Single-Circuit and Double-Circuit Untransposed Lines Based on Redundant Measurements

Fault type	Fault Loca. (p.u.)	Fault res. (Ω)	Est. error (%)	
			Single-circuit case	Double-circuit case
AG	0.3	1	0.03	0.03
		5	0.17	0.04
		50	0.05	0.05
	0.8	1	0.04	0.02
		5	0.04	0.02
		20	0.05	0.05
BC	0.3	1	0.11	0.03
		10	0.09	0.04
		20	0.13	0.03
	0.6	1	0.08	0.03
		10	0.08	0.03
		50	0.13	0.01
BCG	0.3	1	0.04	0.04
		5	0.04	0.05
		50	0.05	0.08
	0.7	1	0.09	0.03
		5	0.07	0.04
		50	0.00	0.06
ABC	0.2	1	0.00	0.08
		5	0.02	0.15
		50	0.04	0.09
	0.6	1	0.01	0.06
		5	0.02	0.02
		50	0.22	0.07

2.4.2 Optimal Estimator Evaluation

This case study illustrates how to detect and identify bad measurements with the proposed optimal estimator. In our study, the voltage measurements from buses 3, 8, 10 and 13 are utilized to obtain the fault location. A value of 1e-4 is chosen for the variance for the voltage measurements, and a value of 1e-6 is chosen for the variance for other measurements.

Table 2.6 Optimal Estimates with Presence of Bad Data

Quantity	Unit	Actual Value	Optimal Estimate
$\lvert\Delta V_{3a}\rvert$	p.u.	0.3566	0.4702
$\angle\Delta V_{3a}$	rad	-3.0908	-3.0845
$\lvert\Delta V_{8a}\rvert$	p.u.	0.6116	0.6257
$\angle\Delta V_{8a}$	rad	-3.0828	-3.0844
$\lvert\Delta V_{10a}\rvert$	p.u.	0.3887	0.4003
$\angle\Delta V_{10a}$	rad	-3.1258	-3.1279
$\lvert\Delta V_{13a}\rvert$	p.u.	0.2841	0.3076
$\angle\Delta V_{13a}$	rad	-3.1362	-3.1400
Fault Location	p.u.	0.8	0.6851

Table 2.7 Optimal Estimates with Bad Data Removed

Quantity	Unit	Actual Value	Optimal Estimate
$\lvert\Delta V_{8a}\rvert$	p.u.	0.6116	0.6122
$\angle\Delta V_{8a}$	rad	-3.0828	-3.0830
$\lvert\Delta V_{10a}\rvert$	p.u.	0.3887	0.3887
$\angle\Delta V_{10a}$	rad	-3.1258	-3.1258
$\lvert\Delta V_{13a}\rvert$	p.u.	0.2841	0.2837
$\angle\Delta V_{13a}$	rad	-3.1362	-3.1364
Fault Location	p.u.	0.8	0.7977

Suppose that an AG fault occurs on line from bus 4 to bus 6 with the actual fault location being 0.8 p.u. and the fault resistance as 5 ohms. Suppose that there is an error of 50% in the superimposed voltage magnitude measurement at phase A at bus 3.

The optimal estimation result with presence of the bad data is shown in Table 2.6. Only phase A voltage estimate of each bus and the estimated fault location are listed here.

In this care, $h = 35$ and $\chi^2_{35,0.01} = 57.342$, with α being chosen as 0.01. The estimated value of the cost function is calculated as 122.709, which is greater than $\chi^2_{35,0.01}$. Thus, the presence of bad data is suspected. To identify the bad measurement, the normalized error is computed, and the largest value corresponds to the magnitude of the superimposed voltage at phase A at bus 3.

Hence the phase A voltage measurement at bus 3 is identified as the bad measurement.

To eliminate the effect of bad measurement, the voltage measurements at bus 3 are discarded. After that, the estimator calculates a new set of optimal estimates. In this scenario, the expected value of cost function is 17, and $\chi^2_{17,0.01} = 33.409$. The newly estimated value of cost function is 0.040, which is much less than $\chi^2_{17,0.01}$. So all of the measurements are considered as acceptable. The re-estimated results by the optimal estimator are listed in Table 2.7. The fault location percentage error is calculated as 0.23%. It is shown that the fault location estimate is significantly enhanced.

2.5 Summary

Most of the previous fault location methods require measurements taken from terminals of the faulted line. Those algorithms using wide area measurements require fault type information and do not model untransposed lines precisely.

This chapter proposes fault location methods for untransposed transmission lines by utilizing sparse wide area measurements. The methods are applicable to both single-circuit and double-circuit transmission lines, and are immune to fault resistances. In addition, the fault type information is not a

prerequisite. The shunt capacitance of transmission line is fully considered based on the distributed parameter line model. When synchronized measurements from multiple buses are available, an optimal estimator is proposed. The estimator is able to detect and identify possible measurement errors, and remove them to enhance estimation. It is noted that the proposed methods still provide quite accurate results when measurements from only one bus are available.

Evaluation studies have demonstrated that the proposed algorithms can yield quite accurate estimates under various fault conditions for both single- and double-circuit untransposed lines.

Chapter 3 Location of Evolving Faults in Transmission Systems Based on Sparse Wide-Area Measurements

3.1 Introduction

In Chapter 2, a wide-area fault location method that is applicable to both transposed and untransposed lines is proposed. The fault types considered in Chapter 2 are principal fault types, including LG fault, LL fault, LLG fault, LLL fault and LLLG fault. The fault type during a fault period is assumed to be unchanged.

In electric power systems, however, not all fault conditions remain unchanged during faults. Evolving faults are types of faults such that the faulted phases change over time [43]. Evolving faults occur less often than commonly occurring shunt faults (LG, LL, LLG, LLL and LLLG faults). However, in post-fault power networks, evolving faults can easily happen since the systems are under abnormal conditions [44], [45].

Locating evolving faults is challenging due to the change in fault type shortly after the fault initiation. Existing studies on locating evolving faults is very limited. This chapter presents a new approach to estimate the locations of evolving faults in transmission lines.

By using sparse wide area voltage measurements, this method can accurately locate evolving faults without requiring measurements from either end of the faulted line. Fault type information is not a necessity either, and the change of fault phases does not affect the estimation accuracy. In addition, the algorithm is applicable to both single-circuit and double-circuit lines, and the transmission lines can be either transposed or untransposed. Distributed parameter line model is adopted to fully consider the shunt capacitances of the transmission lines. EMTP simulation package is employed to evaluate the method, and quite accurate results have been achieved.

The rest of this chapter is organized as follows: Section 3.2 introduces the background of evolving faults, including the causes of evolving faults, their characteristics, and existing studies on evolving faults. Section 3.3 presents evaluation studies of the proposed locator, followed by the summary in Section 3.4.

3.2 Characteristics of Evolving Faults

An evolving fault is such a fault that the faulted phases change over time [43]. Evolving faults are more complicated compared to the common shunt faults, and are adversary to distance relay's performance.

The characteristic of an evolving fault is that its faulted phases change over time, while other types of faults' faulted phases remain unchanged. Whether a

fault can be referred to as an evolving fault depends on its faulted phase(s), rather than other fault conditions such as fault resistance. For example, a fault with time-dependent fault resistance is not an evolving fault if its faulted phases do not change.

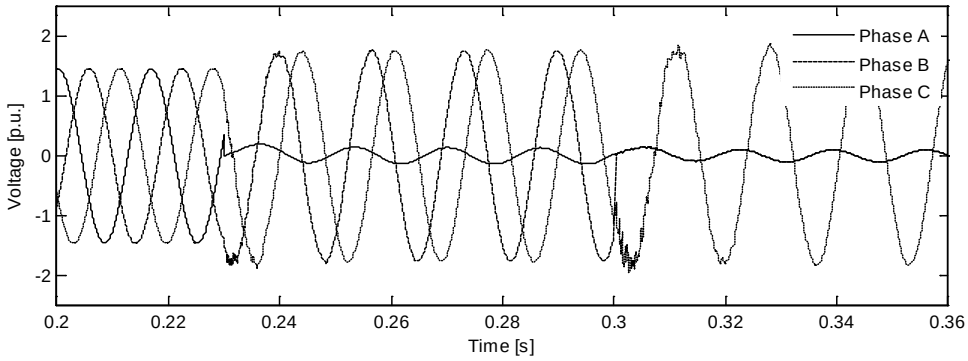

(a)

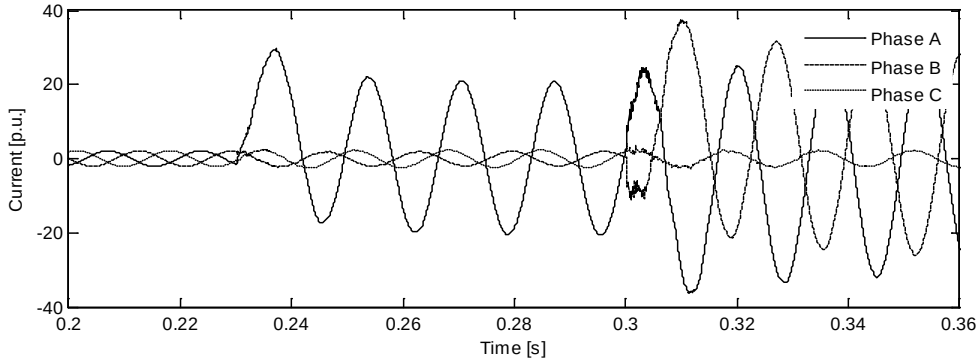

(b)

Figure 3.1 Voltage and current waveforms during an example evolving fault changing from AG-to-ABG fault
(a) Voltage waveform of an example evolving fault
(b) Current waveform of an example evolving fault

Evolving faults can easily happen in overhead systems, when the object causing the initial fault touches conductor(s) of additional phase or phases [44],[46]. For example, an evolving fault may happen when a tree limb first touches one, then two phases in succession, making the fault changes from single line-to-ground fault to double line-to-ground fault [47].

Figure 3.1 depicts the voltage and current waveform of an example evolving fault. The fault initially occurs at as a single line-to-ground fault in phase A, and evolves to a double line-to-ground fault between phases A and B within around four cycles. Typically, the location of an evolving fault would not change during the fault period [45].

There have been several articles discussing evolving faults in transmission grid [45]-[49]. The authors of [45] use the ratio of zero sequence fault current over negative sequence fault current as the criterion to detect evolving faults. In [46], a few evolving faults recorded by transmission line relays are presented. It is learned from these practical experiences that evolving faults can delay distance element tripping which may result in longer duration of existence of faults. Due to evolving fault's changing nature, fault classification is not easy. In [48], the impact of evolving fault on the fault phase selector is analyzed, and it is shown that various factors such as fault position and fault resistance could cause incorrect phase

selection. The authors of [49] use artificial neural networks (ANN) to select fault phase of evolving faults.

There are very few literatures discussing fault location during evolving faults. Reference [44] presents a time-domain method to locate evolving faults in distribution systems. This method requires accurate fault classification that is a demanding task itself. Incorrect fault classification would yield erroneous estimation of where the fault happens. In [47], a method based on ANN is designed to locate evolving faults on transmission lines without knowing fault type information, where the network is trained under a variety of possible fault conditions.

3.3 Location Method for Evolving Faults

The location method is also based on bus impedance matrix concepts, and adopts the core equations of the method in Chapter 2. To deal with evolving faults, the fault locator should continuously determine the estimates of locations from the inception of an evolving fault, and generates a locus of fault location.

In the faulted network, a fictitious bus is added at the assumed fault point. A fictitious bus added on a single-circuit line incorporates three nodes, while a fictitious bus added on a double-circuit line consists of six nodes.

The pre-fault network's bus impedance matrix is assumed to be known. The transfer impedances between the faulted nodes and an arbitrary node, as well as

the driving point impedances of the faulted nodes, can be determined following a similar procedure as that developed in Chapter 2.

Based on the transfer impedances and the driving point impedances, the during-fault fault current and voltage at the fault nodes can be expressed as

$$\boldsymbol{I}_f = -(\boldsymbol{Z}_{kr}{}^T \boldsymbol{Z}_{kr})^{-1}(\boldsymbol{Z}_{kr}{}^T \boldsymbol{\Delta E}_k) \tag{3.1}$$

$$\boldsymbol{E}_r = \boldsymbol{E}_{r0} - \boldsymbol{Z}_{rr}\boldsymbol{I}_f \tag{3.2}$$

where,

$\boldsymbol{\Delta E}_k$ superimposed voltage at a measurable bus k;

$\boldsymbol{E}_{r0}$ pre-fault voltage at the fault bus, which can be estimated based on the pre-fault condition

Based on $\boldsymbol{I}_f$ and $\boldsymbol{E}_r$, the reactive power consumed by the fault resistance can be computed as

$$Q = \text{Imag}\left\{-\boldsymbol{E}_r[(\boldsymbol{Z}_{kr}{}^T \boldsymbol{Z}_{kr})^{-1}(\boldsymbol{Z}_{kr}{}^T \boldsymbol{\Delta E}_k)]^*\right\} \tag{3.3}$$

The unknown fault location is the only unknown variable in (3.3). Since the fault resistance only consumes real power, (3.3) should equal to zero. The fault location can then be solved iteratively.

3.4 Evaluation Studies

The presented fault-location algorithm has been validated by using the Electromagnetic Transients Program (EMTP) simulation data of faults in a 27-bus, 345-kV, 60 Hz transmission system. The diagram of the studied system is shown in Figure 2.2. The bus numbers are labelled besides corresponding buses, and the line lengths in miles are given in parenthesis. Matlab is utilized to implement the proposed methods.

3.4.1 Locating Evolving Faults on Untransposed Single-Circuit Line

The transmission line between bus 4 and bus 6 is an untransposed single-circuit line. A CG-ACG evolving fault occurs 45.72 miles (0.4 p.u.) away from the bus 4. The evolving fault starts as a CG fault on 0.1s, and evolves into ACG fault approximately two cycles later. The voltage measurements from bus 8, as shown in Figure 3.2, are recorded and used to locate the evolving fault. It can be observed that the Phase C voltage decreases from the initial-stage of the evolving fault, and both Phase A and Phase C voltages drop below normal values in the second-stage. The fault location algorithm developed in Section 3.3 is applied to estimate the fault location 8. The locus of estimated fault location over time is depicted in Figure 3.3. The estimated location locus levels off at 0.4 after the initial fluctuation. Due to the transients introduced by the fault type transition, the locus oscillates around

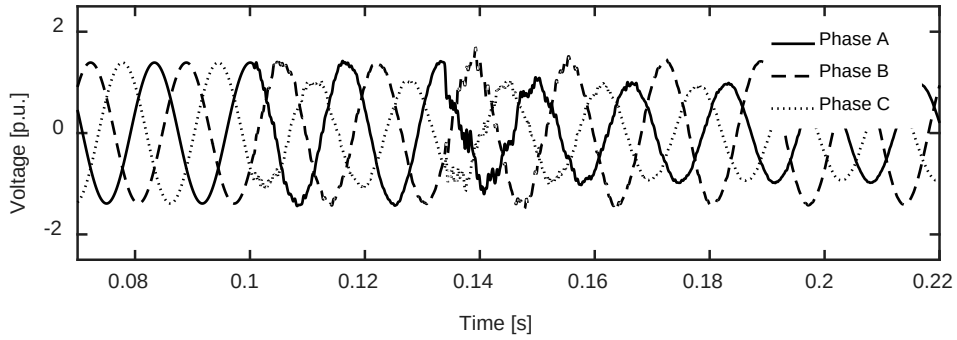

Figure 3.2 Voltage measurements from bus 8 during a CG-ACG evolving fault on an untransposed single-circuit line

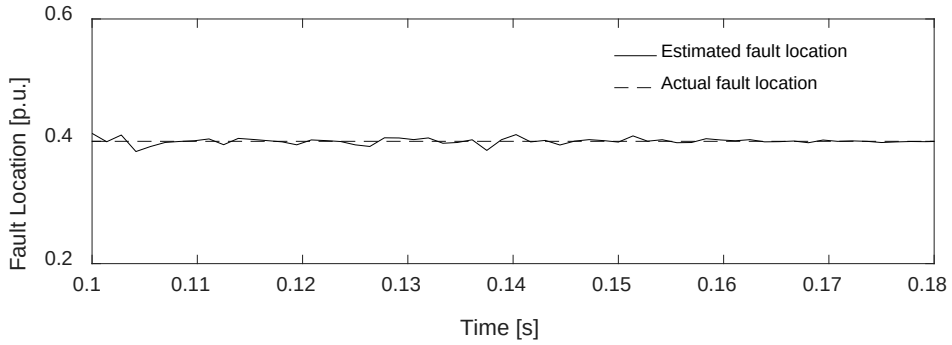

Figure 3.3 Fault location estimation locus of the AG-ACG evolving fault on an untransposed single-circuit line

0.14s. Afterwards, the locus coincides with the actual fault location reference line quickly. The proposed location algorithm yields considerably accurate fault location results over time.

3.4.2 Locating Evolving Faults on Transposed Single-Circuit Line

The transmission line between bus 4 and bus 10 is a transposed single-circuit line. An evolving fault occurs on this transmission line. Assume the voltage measurements from bus 21 is available, as shown in Figure 3.4, and the

measurements are used to locate the evolving fault. The studied fault is 0.7 p.u. away from the bus 4.

The initial stage of the evolving fault lasts from 0.1 s to 0.13 s. It can be observed that only BCG fault exists during this stage, since only the Phase B's and Phase C's voltages decrease. In the rest period of the event, the fault evolves into ABCG fault, where all three phases' voltage drop significantly. At the beginning period of the fault inception and fault type evolution, the location locus oscillates due to inaccuracy in phasor estimation. However, even with these errors, the fault location estimation is still quite reliable. The locus of the fault location versus time is drawn in Figure 3.5.

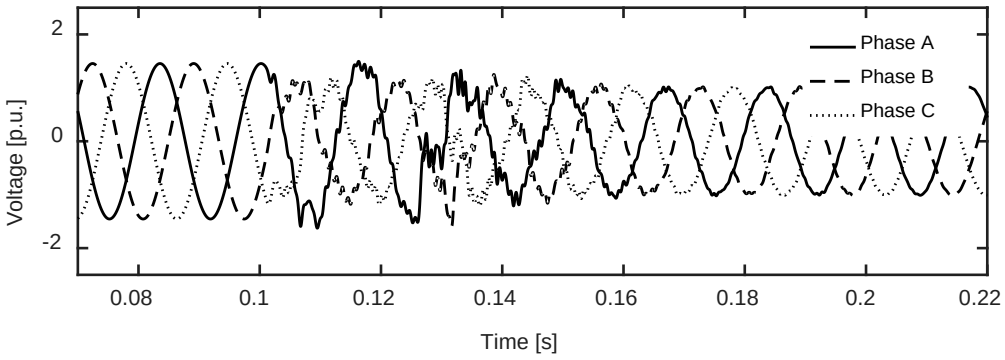

Figure 3.4 Voltage measurements from bus 21 during a BCG-ABCG evolving fault on a transposed single-circuit line

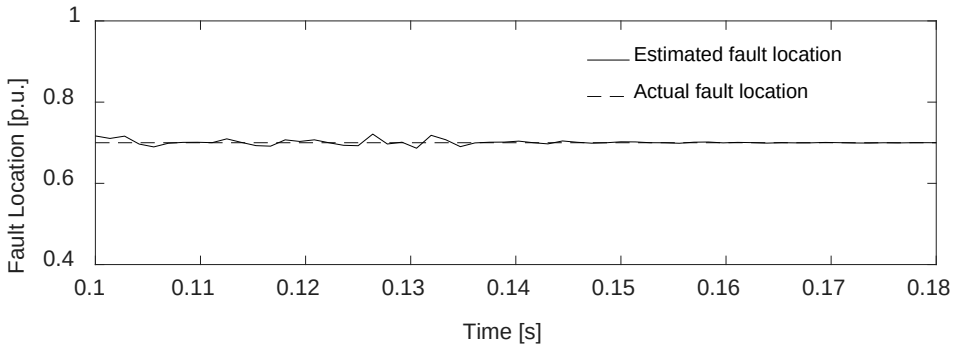

Figure 3.5 Fault location estimation locus of the BCG-ABCG evolving fault on a transposed single-circuit line

3.4.3 Locating Evolving Faults on Untransposed Double-Circuit Line

An evolving fault occurs on the double-circuit untransposed transmission line between bus 9 and bus 10. The voltage measurements from bus 22 is used for locating the fault which occurs 67.28 miles, i.e. 0.4 p.u., away from bus 9. The fault starts as AG fault and evolves into ABCG fault after around 1.5 cycle. The voltage measurements at bus 5 are shown in Figure 3.6.

Figure 3.7 depicts the estimation locus of the evolving fault's location. Some phasor estimation errors at the transition stage introduces some minor location errors for that period. However, it can be observed that quite accurate fault location result is then quickly achieved. The locus of the fault location can help researchers and engineers to better understand the nature of the studied fault.

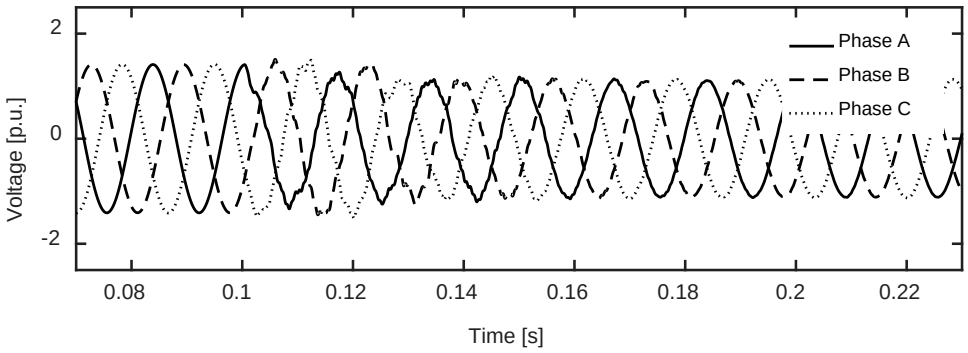

Figure 3.6 Voltage measurements from bus 22 during an AG-ABCG evolving fault on an untransposed double-circuit line

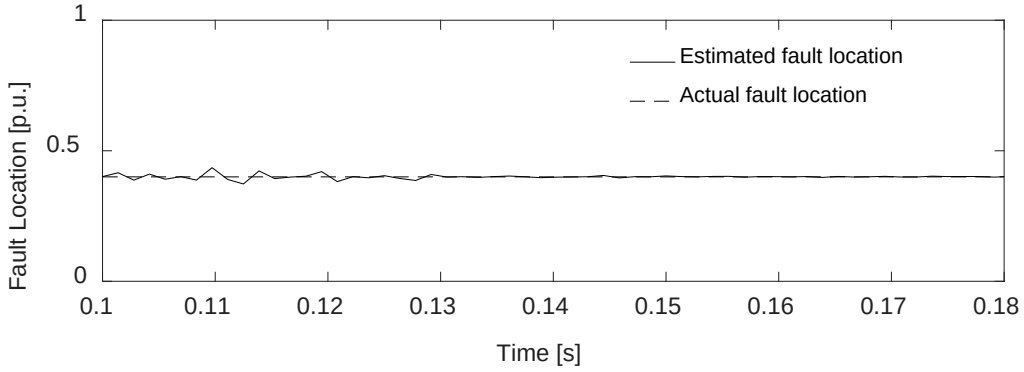

Figure 3.7 Fault location estimation locus of the AG-ABCG evolving fault on an untransposed double-circuit line

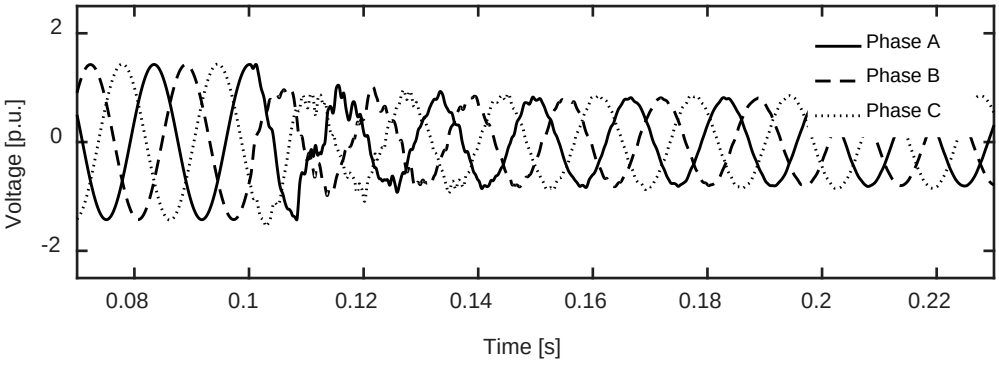

Figure 3.8 Voltage measurements from bus 15 during a BG-ABCG evolving fault on a transposed double-circuit line

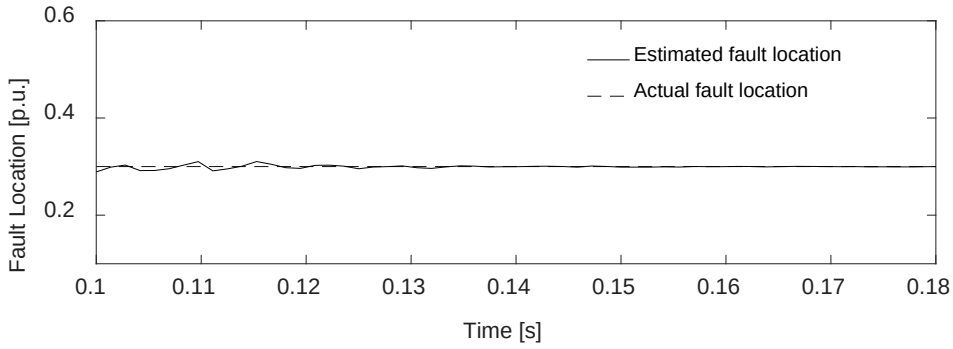

Figure 3.9 Fault location estimation locus of the BG-ABCG evolving fault on an untransposed double-circuit line

3.4.4 Locating Evolving Faults on Transposed Double-Circuit Line

Assume the double-circuit line between bus 9 and bus 10 is transposed. An example evolving fault is assumed to evolve from BG fault to ABCG fault 8 ms after the initial fault. The fault resistance is 5 ohms, and the actual fault location is 0.3 p.u. away from the bus 9. Figure 3.8 depicts the voltage measurement from bus 15. The fault location estimation locus is drawn in Figure 3.9. The estimation locus first oscillates around the reference line that represents the actual fault location. Afterwards, the estimation locus and the reference line up with each other. In other words, quite accurate estimation is yielded.

In the cases presented above, four different types of transmission lines suffer from different types of evolving fault with various fault resistances. However, quite satisfactory location results can be obtained based on the proposed method, regardless of what the fault conditions and line types are. In addition, the

availability of fault location locus over time can help utility engineers enhance awareness of events in power systems, and help understand the nature and evolution of the studied faults.

3.4.5 Numerical Fault Location Results

The previous parts of this section present recorded voltage waveform and graphical fault location results in the form of estimation locuses. This part exhibits numeric fault location results tested under a variety of fault conditions. Evolving fault happening on single-circuit and double-circuit lines are included in the study. Both transposed and untransposed lines are used to evaluate the algorithm.

Table 3.1-Table 3.4 summarizes representative results. In these tables, the first columns give the fault types of the initial stages of evolving faults, while the second columns list the fault types of the second stage of the evolving faults. The fault resistances of the initial and second stages are given in Column Three and Columns Four, respectively. A variety of fault type changes have been studied, such as faults evolve from single line to ground faults to double line to ground faults, etc. The fault resistances may or may not change during the entire period of faults. Columns Five gives the actual fault location in per unit. The time intervals between the inception of the initial stage and the second stage are presented in the sixth columns.

Table 3.1 Location Results for Evolving Faults on Untransposed Single-Circuit Lines

Ini. fault type	**Sec. fault type**	**Ini. fault res. (Ω)**	**Sec. fault res. (Ω)**	**Fault loca. (p.u.)**	**Time inter-val (ms)**	**Est. error(%) based on meas. from bus**	
						7	*19*
AG	ABG	1	1	0.3	15	0.01	0.05
CG	BCG	5	5	0.2	20	0.11	0.19
AG	ACG	1	5	0.5	30	0.03	0.12
BG	BCG	10	10	0.7	26	0.15	0.07
BG	ABCG	5	5	0.6	8	0.02	0.02
CG	ABCG	20	20	0.3	17	0.13	0.19
AC	ABC	5	15	0.7	17	0.06	0.08
BC	ABC	1	10	0.8	10	0.19	0.06
AB	ABC	1	1	0.1	10	0.05	0.05
BC	ABC	15	5	0.5	15	0.07	0.09
ACG	ABCG	15	10	0.5	15	0.12	0.13
ABG	ABCG	10	10	0.9	50	0.08	0.04
BCG	ABCG	20	20	0.9	50	0.22	0.15
ACG	ABCG	1	1	0.2	30	0.01	0.01

Table 3.2 Location Results for Evolving Faults on Transposed Single-Circuit Lines

Ini. fault type	**Sec. fault type**	**Ini. fault res. (Ω)**	**Sec. fault res. (Ω)**	**Fault loca. (p.u.)**	**Time inter-val (ms)**	**Est. error(%) based on meas. from bus**	
						3	*21*
AG	ABG	10	10	0.4	26	0.14	0.06
AG	ACG	1	1	0.3	17	0.07	0.03
BG	BCG	25	25	0.5	30	0.15	0.18
BG	ABG	30	30	0.5	10	0.16	0.21
CG	ACG	10	15	0.7	35	0.05	0.06
CG	BCG	5	5	0.2	20	0.09	0.07
AG	ABCG	50	50	0.8	15	0.13	0.22
CG	ABCG	20	20	0.1	7	0.09	0.09
BC	BCG	1	1	0.1	35	0.01	0.01
AB	ABG	15	10	0.6	40	0.05	0.09
AC	ACG	5	5	0.9	30	0.03	0.03
BCG	ABCG	15	20	0.4	15	0.10	0.18
ABG	ABCG	5	15	0.3	10	0.02	0.17
ACG	ABCG	10	10	0.6	20	0.05	0.09

Table 3.3 Location Results for Evolving Faults on Untransposed Double-Circuit Lines

Ini. fault type	**Sec. fault type**	**Ini. fault res. (Ω)**	**Sec. fault res. (Ω)**	**Fault loca. (p.u.)**	**Time inter-val (ms)**	**Est. error(%) based on meas. from bus**	
						13	*25*
AG	ABG	1	10	0.2	26	0.05	0.08
AG	ACG	15	5	0.8	10	0.04	0.12
CG	ACG	10	10	0.6	10	0.08	0.09
CG	ABCG	15	15	0.3	15	0.05	0.12
BG	ABCG	5	5	0.3	30	0.09	0.06
BG	ABG	20	10	0.3	40	0.09	0.11
BC	BCG	10	10	0.7	40	0.03	0.04
BC	ABC	50	50	0.5	25	0.22	0.21
AB	ABG	30	30	0.2	15	0.15	0.09
AB	ABC	25	15	0.4	8	0.17	0.08
ABG	ABCG	1	1	0.1	8	0.02	0.03
ACG	ABCG	5	5	0.2	20	0.07	0.06
BCG	ABCG	15	10	0.8	20	0.04	0.05
ABC	ABCG	20	10	0.9	15	0.02	0.03

Table 3.4 Location Results for Evolving Faults on Transposed Double-Circuit Lines

Ini. fault type	**Sec. fault type**	**Ini. fault res. (Ω)**	**Sec. fault res. (Ω)**	**Fault loca. (p.u.)**	**Time inter-val (ms)**	**Est. error(%) based on meas. from bus**	
						11	*22*
BG	ABCG	20	25	0.1	15	0.15	0.11
AG	ABCG	50	50	0.8	20	0.19	0.22
AC	ACG	1	1	0.9	10	0.03	0.05
AC	ABCG	5	5	0.3	5	0.05	0.09
BC	BCG	10	10	0.3	30	0.05	0.08
BC	ABCG	15	15	0.4	40	0.07	0.06
ABC	ABCG	20	20	0.5	15	0.02	0.15
AB	ABC	15	5	0.5	17	0.05	0.12
CG	ACG	1	5	0.6	26	0.08	0.08
CG	ABCG	10	15	0.2	10	0.02	0.03
BCG	ABCG	10	10	0.7	10	0.12	0.17
ABG	ABCG	5	15	0.7	30	0.00	0.02
AB	ABG	1	1	0.4	50	0.05	0.04
ACG	ABCG	20	20	0.1	8	0.12	0.15

3.5 Summary

Transmission lines are prone to evolving faults in addition to common shunt short-circuit faults. Evolving fault are types of faults such that the faulted phases change over time. Such kind of faults can easily happen in overhead systems, when the object causing the initial fault touches conductor(s) of additional phase or phases. Due to un-stationary fault conditions, it is not easy to determine the fault types and thus their locations. Little existing literatures discuss location of evolving faults.

To complement such gap, this chapter extends the method developed in Chapter 2 to locate evolving faults on transmission lines. Compare with location methods based on soft computing, the proposed method does not require an extensive amount of data for training. The method makes use of sparse wide area measurements taken by PMUs. These measurements are not necessarily captured from either end of the faulted transmission line. The proposed method is applicable to both single-circuit and double-circuit transmission lines, and the lines can be either transposed or untransposed. Evaluation studies show that the proposed methods yield quite accurate results. The proposed algorithm has a good potential to help utility engineers and researchers to protect and recover power systems from evolving faults.

Chapter 4 Location of Inter-Circuit Faults on Double-Circuit Transmission Lines Based on Sparse Wide-Area Measurements

4.1 Introduction

An evolving fault, although its faulted phases changes over time, is still considered as a single fault. In addition to single faults, simultaneous faults may also occur in a transmission system. A simultaneous fault refers to a combination of two or more faults at the same time [50].

Inter-circuit fault is a type of simultaneous fault, and it is the most common simultaneous fault type [50]. An inter-circuit fault occurs at a single geographical location, and connects two or more circuits [51], [52]. The conductor geometry of multi-circuit lines makes them prone to inter-circuit faults, and the probability of inter-circuit faults increases when multiple lines are mounted on the same tower [53]. In addition to multi-circuit lines, an inter-circuit fault may also occur between single-circuit lines when they share the same tower structure.

The causes of inter-circuit faults can be various. Lighting, bush fires under lines, falling of tree limbs, accidental conductor contact, etc. may all cause inter-circuit faults [53]-[56]. Many inter-circuit faults on double-circuit lines occur as results of lightning. When a lightning strike hits a transmission tower or an earth

wire, the tower potential raises, and the backflash may cause an inter-circuit fault connecting two circuits [54], [57]. The likelihood of such condition is high when the tower footing resistance is high, e.g. in a rocky area [57]. The number of inter-circuit faults causes by backflash can be reduced by making sure that earth wires are over-run with small shielding angles, and that the tower earth resistances are kept low.

Inter-circuit faults between each circuit in a double-circuit line is the most common inter-circuit fault [50]. Such a fault occurs when phases of each circuit are connected through objects such as electric arc and tree limb. Earth may or may not involves in such faults. During unearthed inter-circuit fault, the fault path does not include ground, but zero-sequence current is still present, which make phase selection problematic [58]. Inter-circuit faults can cause serious system instability when phase and ground relaying schemes are used for protection, because they will trip three phases of both circuits [59].

The authors of [53] presents an artificial neural network based method to detect and classify inter-circuit faults. The authors of [60] propose a new fault-loop impedance measurement algorithm for inter-circuit faults on double-circuit lines. Reference [51] analyzed an inter-circuit fault in a 138 kV system, and concluded several lessons learned, such as that the traditional criteria to detect a three-phase fault to block reclosing based on negative sequence components may not work for

complex faults. In [55], different protection schemes are evaluated for inter-circuit fault conditions. McDaniel analyzed an inter-circuit fault between a 161 kV transmission line and an underbuilt 69 kV sub-transmission line, and proposed two fault location methods which both require local measurements [61]. A location method of inter-circuit faults is proposed in [62]. The algorithm is based on generalized fault-loop model, and requires fault type information. The inter-circuit faults studied in [62] are those that connect one phase in each circuit, and the inter-circuit faults that involve multiple phases are not considered.

This chapter proposes a new location method for inter-circuit faults based on sparse wide-area measurements. The proposed fault location method omits the necessity to identify fault types. Sparse wide area measurements, which may be taken from buses far away from the faulted line, are utilized by the proposed method instead of local measurements. The proposed algorithm is derived in phase-domain, and is applicable to both transposed and untransposed transmission lines. Distributed parameter line model is utilized in order to fully consider the shunt capacitances. The rest of the chapter is organized as follows: Section 4.2 illustrates the proposed fault location algorithm. Section 4.3 presents the evaluation studies, followed by the conclusion.

4. 2 Location Algorithm for Inter-Circuit Faults on Double-Circuit Transmission Lines

This section presents a wide-area location method for inter-circuit faults on double-circuit transmission lines based on sparse wide-area measurements.

In modern power systems, it is quite often to find double-circuit lines transmitting power in narrow physical corridors. There are also places in power systems where single-circuit lines are mounted on a same tower. An inter-circuit fault may occur in both situations.

Figure 4.1 depicts several examples of inter-circuit faults. E_P, E_P, E_P and E_P represents the Thevenin equivalent sources. Figure 4.1 (a) presents the one-line diagram of a double-circuit transmission line with an inter-circuit fault. Two fictitious buses, bus *R* and bus *S*, are added at the assumed inter-circuit fault location as shown in Figure 4.1. But *R* contains nodes R_1, R_2 and R_3. Bus *S* contains nodes R_1, R_2 and R_3. Bus *P* and bus *Q* are the studied line's the starting and ending bus, respectively, each of which contains six nodes. Figure 4.1 (b) exhibits an inter-circuit fault between two single-circuit lines with the same voltage level. Figure 4.1 (c) is an example inter-circuit fault between two lines with different voltage levels.

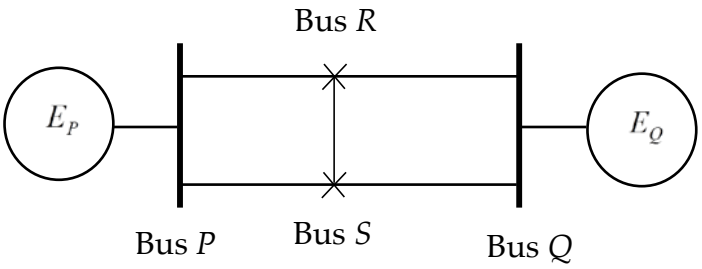

(a)

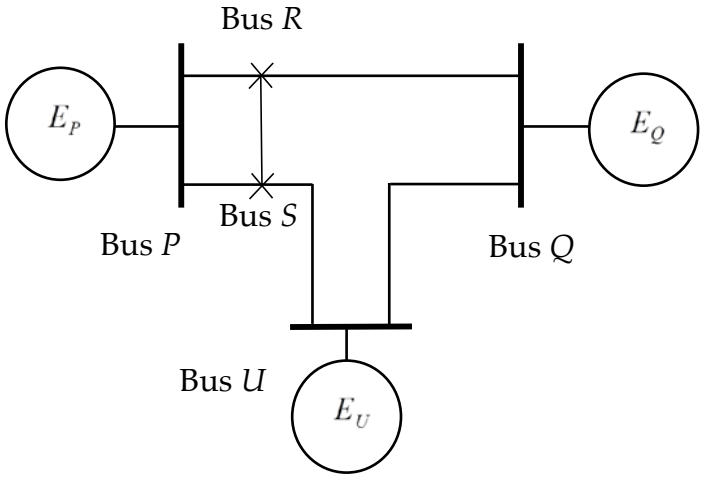

(b)

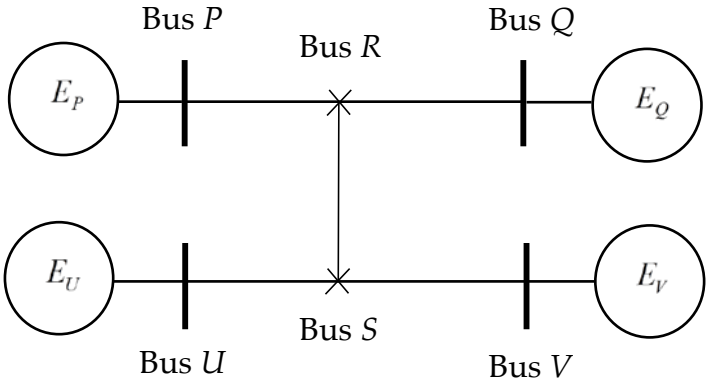

(c)

Figure 4.1 Examples of inter-circuit faults

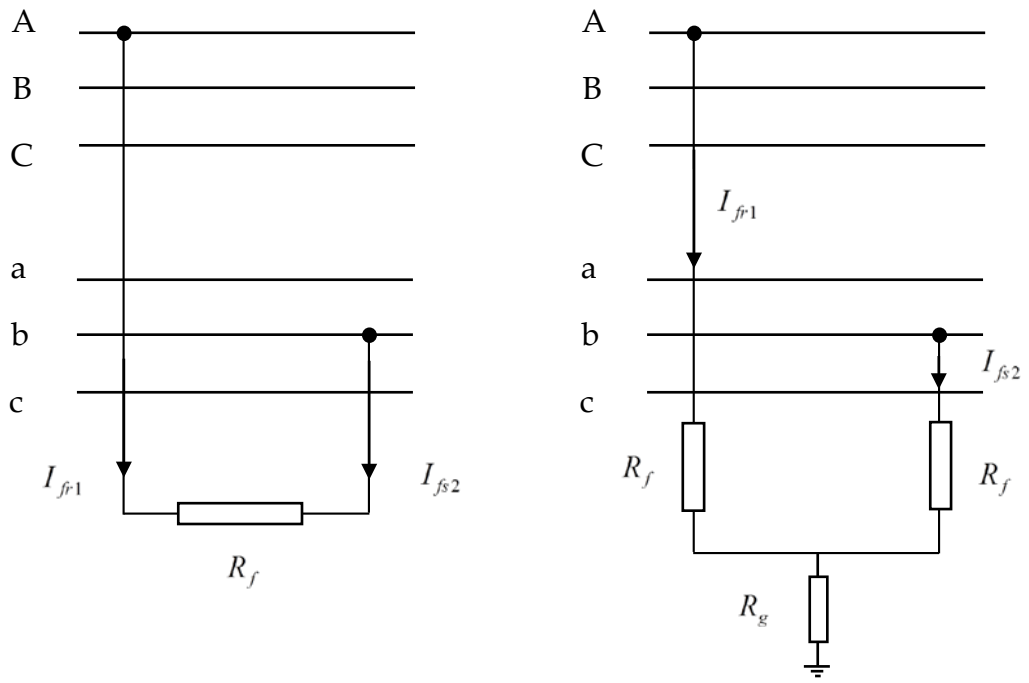

Figure 4.2 Models of (a) an unearthed ICF, and (b) an earthed ICF.

To illustrate the mechanism of inter-circuit faults clearly, Figure 4.2 depicts the models of an unearthed and an earthed inter-circuit faults involving phase A and phase B. Assume $\boldsymbol{I}_{\boldsymbol{fr}}$ and $\boldsymbol{I}_{\boldsymbol{fs}}$ are the fault current vectors involving bus *R* and bus *S*, respectively. The fault currents can be expressed as

$$\boldsymbol{I}_{\boldsymbol{fr}} = [I_{fr_1}, I_{fr_2}, I_{fr_3}]^T \tag{4.1}$$

$$\boldsymbol{I}_{\boldsymbol{fs}} = [I_{fs_1}, I_{fs_2}, I_{fs_3}]^T \tag{4.2}$$

where $[.]^T$ represents transpose of a matrix. If a phase *i* is not the faulted phase, then the corresponding fault current I_{fr_i} or I_{fs_i} equals to zero.

Assume bus k and bus l are two measurable buses in the transmission system except the fictitious buses. Based on the superimposed theory and the meaning of transfer impedance, the voltage change due to the inter-circuit fault, i.e. the superimposed voltage at bus k and bus l, can be written as

$$\boldsymbol{\Delta E}_k = -\boldsymbol{Z}_{kr}\boldsymbol{I}_{fr} - \boldsymbol{Z}_{ks}\boldsymbol{I}_{fs} \tag{4.3}$$

$$\boldsymbol{\Delta E}_l = -\boldsymbol{Z}_{lr}\boldsymbol{I}_{fr} - \boldsymbol{Z}_{ls}\boldsymbol{I}_{fs} \tag{4.4}$$

where $\boldsymbol{\Delta E}_k$ is the superimposed voltage at bus k, $\boldsymbol{\Delta E}_l$ is the superimposed voltage at bus l, $\boldsymbol{Z}_{kr}$ is the transfer impedance matrix between bus k and bus r, $\boldsymbol{Z}_{ks}$ is the transfer impedance matrix between bus k and bus s, $\boldsymbol{Z}_{lr}$ is the transfer impedance matrix between bus l and bus r, $\boldsymbol{Z}_{ls}$ is the transfer impedance matrix between bus l and bus s. The superimposed voltages at bus k and bus l can be measured by using PMUs. The transfer impedances can be expressed as functions of unknown fault distance. The transfer impedances can be derived following a similar procedure to that in Chapter 2.

Note that the studied parallel lines in this chapter have identical parameters. Therefore, it holds that

$$\boldsymbol{Z}_{kr} = \boldsymbol{Z}_{ks} \tag{4.5}$$

$$\boldsymbol{Z}_{lr} = \boldsymbol{Z}_{ls} \tag{4.6}$$

Equations (4.3) and (4.4) can be re-written as

$$\Delta \boldsymbol{E}_k = -\boldsymbol{Z}_{kr}(\boldsymbol{I}_{fr} + \boldsymbol{I}_{fs}) = -\boldsymbol{Z}_{kr}\boldsymbol{I}_{f_{sum}} \tag{4.7}$$

$$\Delta \boldsymbol{E}_l = -\boldsymbol{Z}_{lr}(\boldsymbol{I}_{fr} + \boldsymbol{I}_{fs}) = -\boldsymbol{Z}_{lr}\boldsymbol{I}_{f_{sum}} \tag{4.8}$$

It follows from (4.7) and (4.8) that

$$\boldsymbol{I}_{f_{sum}} = -(\boldsymbol{Z}_{kr}{}^T\boldsymbol{Z}_{kr})^{-1}(\boldsymbol{Z}_{kr}\Delta \boldsymbol{E}_k) \tag{4.9}$$

$$\boldsymbol{I}_{f_{sum}} = -(\boldsymbol{Z}_{lr}{}^T\boldsymbol{Z}_{lr})^{-1}(\boldsymbol{Z}_{lr}\Delta \boldsymbol{E}_l) \tag{4.10}$$

Eliminating $\boldsymbol{I}_{f_{sum}}$ from (4.9) and (4.10) results in

$$(\boldsymbol{Z}_{kr}{}^T\boldsymbol{Z}_{kr})^{-1}(\boldsymbol{Z}_{kr}\Delta \boldsymbol{E}_k) - (\boldsymbol{Z}_{lr}{}^T\boldsymbol{Z}_{lr})^{-1}(\boldsymbol{Z}_{lr}\Delta \boldsymbol{E}_l) = 0 \tag{4.11}$$

Since the transfer impedances in (4.11) are functions of fault location, and the superimposed voltages can be measured, (4.11) only includes one unknown variable. Thus, the fault location can be derived.

If the measurements at bus *k* and bus *l* are unsyncrhonized, by equaling the magnitudes of (4.9) and (4.10), the fault location can still be obtained by solving the following equation:

$$|(\boldsymbol{Z}_{kr}{}^T\boldsymbol{Z}_{kr})^{-1}(\boldsymbol{Z}_{kr}\Delta \boldsymbol{E}_k)| - |(\boldsymbol{Z}_{lr}{}^T\boldsymbol{Z}_{lr})^{-1}(\boldsymbol{Z}_{lr}\Delta \boldsymbol{E}_l)| = 0 \tag{4.12}$$

Note that whether an inter-circuit fault is earthed or not does not affect the derivation of the fault location. In addition, fault type information is not required by the proposed method. Considering that fault type identification can be challenging for inter-circuit faults, omitting fault classification is an outstanding advantage of the proposed algorithm.

4.3 Evaluation Studies of Inter-Circuit Fault Location

The proposed location method has been validated based on simulation in Electromagnetic Transients Program (EMTP). The 27-bus, 345 kV, 60 Hz system used in Chapter 2 is adopted to model the transmission network. The transmission line between bus 9 and bus 10 is double-circuit line. Inter-circuit faults are supposed to occur on this line. Matlab is utilized to implement the proposed methods.

A variety of inter-circuit faults have been simulated with different fault conditions, including fault types, resistances, and locations. Representative fault location results are presented as follows:

Table 4.1 exhibits location results for inter-circuit faults on a transposed double-circuit line based on synchronized measurements. Table 4.2 presents location estimates of faults on a transposed double-circuit line obtained using unsynchronized measurements.

Table 4.3 and Table 4.4 lists the location results for inter-circuit faults on untransposed double-circuit lines. Estimates in Table 4.3 are calculated based on synchronized measurements, while the results in Table 4.4. are achieved based on unsynchronized measurements. Columns 1-3 of these tables are the fault type information, actual fault location, and fault resistance, respectively.

In the fault type information, capitalized letters represent the phases on one line of the double-circuit line, small letters are the phases on the other line, and 'G' means ground. The other columns are the fault location estimation errors based on measurements from different buses. Fault location is measured from bus 9.

It is observed that quite accurate results are yielded by the proposed algorithms in various conditions and different line configurations.

Table 4.1 Location results of inter-circuit faults on transposed double-circuit lines based on synchronized measurements

Fault type	Actual fault loc. (p.u.)	Fault res. (Ω)	Est. error (%) using measurements from buses		
			8&11	6&19	13&24
a-B	0.3	5	0.02	0.01	0.07
b-C	0.7	10	0.02	0.01	0.09
a-C-G	0.6	20	0.03	0.02	0.09
b-A-G	0.1	50	0.05	0.06	0.12
a-BC	0.2	30	0.07	0.09	0.10
c-A-G	0.6	5	0.05	0.00	0.02
b-AC	0.7	15	0.08	0.09	0.01
ab-C	0.9	10	0.11	0.05	0.07
c-AB-G	0.1	1	0.03	0.14	0.11
c-B-G	0.8	15	0.01	0.00	0.09
a-A-G	0.7	1	0.02	0.01	0.06
a-AB	0.2	5	0.01	0.01	0.07
b-AC-G	0.6	5	0.02	0.02	0.08
bc-AC-G	0.4	10	0.02	0.01	0.07

Table 4.2 Location results of inter-circuit faults on transposed double-circuit lines based on unsynchronized measurements

Fault type	Actual fault loc. (p.u.)	Fault res. (Ω)	Est. error (%) using measurements from buses		
			5&13	9&22	16&27
a-B	0.3	5	0.07	0.03	0.13
b-C	0.7	10	0.20	0.07	0.10
a-C-G	0.6	20	0.21	0.08	0.10
b-A-G	0.1	50	0.19	0.18	0.18
a-C	0.2	20	0.15	0.07	0.09
Ab-C	0.3	5	0.10	0.09	0.13
ab-BC	0.5	15	0.11	0.05	0.19
c-AB-G	0.7	10	0.09	0.05	0.12
c-B-G	0.8	15	0.16	0.08	0.11
a-A-G	0.7	1	0.11	0.06	0.06
a-AB	0.2	5	0.13	0.04	0.03
b-AC-G	0.6	5	0.14	0.06	0.02
bc-AC-G	0.4	10	0.13	0.05	0.02

Table 4.3 Location results of inter-circuit faults on untransposed double-circuit lines based on synchronized measurements

Fault type	Actual fault loc. (p.u.)	Fault res. (Ω)	Est. error (%) using measurements from buses		
			3&12	11&16	15&22
a-A-G	0.6	1	0.03	0.16	0.09
a-B	0.2	50	0.19	0.04	0.19
c-A-G	0.4	10	0.05	0.15	0.13
c-C-G	0.8	20	0.06	0.10	0.12
a-BC	0.7	50	0.03	0.18	0.13
a-BC-G	0.7	10	0.03	0.18	0.12
ab-C-G	0.1	1	0.03	0.10	0.10
bc-AC	0.1	5	0.07	0.08	0.11
c-AB	0.6	10	0.10	0.11	0.15
ac-B-G	0.8	20	0.02	0.16	0.16
a-C	0.7	15	0.09	0.21	0.09
c-AB-G	0.1	1	0.03	0.17	0.02
ab-BC-G	0.2	10	0.12	0.11	0.05

Table 4.4 Location results of inter-circuit faults on untransposed double-circuit lines based on unsynchronized measurements

Fault type	Actual fault loc. (p.u.)	Fault res. (Ω)	Est. error (%) using measurements from buses		
			6&22	4&12	8&19
a-A-G	0.6	1	0.08	0.12	0.04
a-B	0.2	50	0.12	0.07	0.09
c-A-G	0.4	10	0.10	0.01	0.03
c-C-G	0.8	20	0.09	0.01	0.02
a-BC	0.7	50	0.12	0.02	0.07
ab-BC-G	0.2	15	0.17	0.09	0.08
c-AC-G	0.3	20	0.05	0.06	0.09
c-BC-G	0.2	1	0.09	0.12	0.11
ac-B-G	0.1	10	0.14	0.02	0.10
a-BC-G	0.7	10	0.12	0.03	0.07
ab-C-G	0.1	1	0.04	0.02	0.01
bc-AC	0.1	5	0.05	0.01	0.01
ab-BC-G	0.2	10	0.10	0.00	0.03

4.4 Summary

Inter-circuit fault is the most common simultaneous fault type in power systems, and usually occur in multi-circuit lines or between single-circuit line that are on the same tower structure. This chapter proposes a new location method for inter-circuit faults on double-circuit transmission lines. Although fault classification can be challenging for inter-circuit faults, this algorithm can still accurately determine fault locations, since fault type information is not a prerequisite. The proposed method utilizes wide-area voltage measurements that do not have to be taken at buses of faulted lines. In addition, the proposed method can deal with inter-circuit faults that involve multiple phases, and is immune to fault resistances. Whether the studied line is transposed or untransposed does not affect the effectiveness of the proposed algorithm. Shunt capacitances are fully modeled and considered. PMUs are used to measure voltage quantities in the system. Even if the measurements are not synchronized, accurate locations can still be obtained. Evaluation studies based on EMTP simulation have demonstrated that the proposed algorithms can yield quite accurate estimates under a variety of inter-circuit fault conditions.

Chapter 5 Parameter-Free Fault Location Method for Series-Compensated Transmission Lines

5.1 Introduction

Chapter 2 – Chapter 4 presents several wide-area fault location methods. These methods rely on some system information, including transmission line parameters. To make this dissertation more comprehensive, this chapter presents a new fault locator for series compensated transmission lines without requiring line parameter information. Synchronized voltage and current measurements from both ends of the faulted line is utilized. Line parameters, along with fault locations, can be estimated online.

In the past decades, fault location methods without utilizing line parameters and fault location methods for series-compensated lines have been put forward. The authors of [63] design a two-terminal parameter-free transmission line fault locator. Such locator utilizes measurements from both ends, and does not require synchronization. Shunt capacitances are ignored by this algorithm. In [64], a parameter-free fault location method based on distributed parameter line model is proposed. Reference [65] presents a fault location algorithm for series-compensated transmission line. The proposed method utilizes two-terminal unsynchronized voltage and current measurements, and it requires line

parameters information. In [66], a fault location method that is applicable to double-circuit series-compensated line is proposed, and shunt capacitances are also considered. The authors of [67] puts forward a parameter-free fault location algorithm for double-circuit transmission lines using two-end current measurements.

The rest of this chapter is organized as follows: Section 5.2 presents the fault location algorithm. Section 5.3 exhibits evaluation studies, followed by summary.

5.2 Parameter-Free Fault location Algorithm

Consider the transmission line between terminals P and Q to be a transposed line. The series compensation device is installed at the point of C. A fault may occur either to the left side or to the right side of the compensator. in Figure 5.1, E_G and E_H represent Thevenin equivalent circuits.

Assume that the equivalent impedances of all three phases of the series compensator are the same, and equal to Z_{SC}. Since there is no mutual coupling between the phases of series compensators, the compensator's equivalent impedance of each sequence is Z_{SC}.

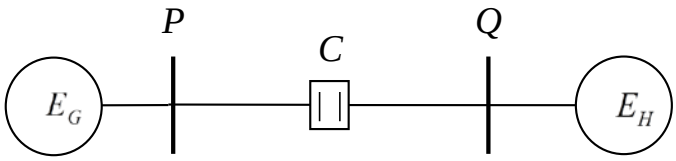

Figure 5.1 Schematic diagram of a series compensated transmission line

Assume that synchronized voltage and current measurements before and during fault are available from both ends. During normal operation, there are N sets of measurements. While during the fault period, only one set of measurements is required. Then, the measurements obtained are

$$\boldsymbol{M} = [V_{P1}, I_{P1}, V_{Q1}, I_{Q1}, ..., V_{PN}, I_{PN}, V_{QN}, I_{QN}, V_{fP}, I_{fP}, V_{fQ}, I_{fQ}] \tag{5.1}$$

where V_{Pi}, I_{Pi}, V_{Qi} and I_{Qi} are the ith set of normal operation measurement, V_{fP}, I_{fP}, V_{fQ} and I_{fQ} are the during-fault measurement.

The unknown variable vector is defined as

$$\boldsymbol{X} = [r^{(1)}, x^{(1)}, b^{(1)}, r^{(0)}, x^{(0)}, b^{(0)}, X_{SC}, m]^T \tag{5.2}$$

where $r^{(1)}, x^{(1)}, b^{(1)}$ are the positive-sequence per-unit series resistance, series reactance, and shunt susceptance; $r^{(0)}, x^{(0)}, b^{(0)}$ are the zero-sequence per-unit series resistance, series reactance, and shunt susceptance; X_{SC} is the per-unit equivalent reactance of the compensator on each sequence; m represents the per-

unit fault location. Therefore, the per-unit equivalent impedance of the compensator on each sequence Z_{SC} is jX_{SC}.

The derivation of measurement vector $\boldsymbol{S}$ and function vector $\boldsymbol{F}(\boldsymbol{X})$ is described as follows:

Based on the equivalent Pi circuit during normal operation as shown in Figure 5.2, the following three equations can be established for sections *PC* and *CQ*:

$$I_{0cL}^{(1)k} = -\frac{1}{Z_C^{(1)}}\sinh(\gamma^{(1)} l_{PC})V_{0P}^{(1)k} + \cosh(\gamma^{(1)} l_{PC})I_{0P}^{(1)k},\ k = 1,\ldots,N \tag{5.3}$$

$$I_{0cR}^{(1)k} = -\frac{1}{Z_C^{(1)}}\sinh(\gamma^{(1)} l_{CQ})V_{0Q}^{(1)k} + \cosh(\gamma^{(1)} l_{CQ})I_{0Q}^{(1)k},\quad k = 1,\ldots,N \tag{5.4}$$

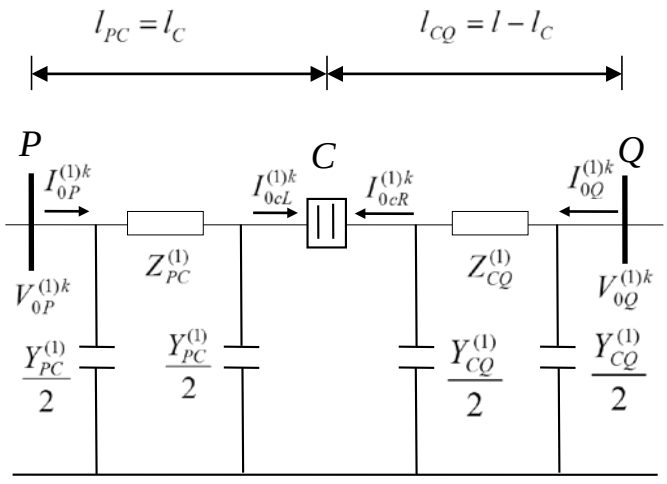

Figure 5.2 Positive-sequence equivalent Pi circuit of series compensated transmission line during normal operation

$$I_{0cL}^{(1)k} = -I_{0cR}^{(1)k}, \quad k = 1,\ldots,N \tag{5.5}$$

where k is the index of set of pre-fault measurements; l is the distance between terminal P and terminal Q; l_C is the distance between terminal P and the compensator location C; $V_{0P}^{(1)k}$ and $V_{0Q}^{(1)k}$ are the kth positive-sequence voltage phasor measurements at P and Q preceding fault, respectively; $I_{0P}^{(1)k}$ and $I_{0Q}^{(1)k}$ are the kth positive-sequence current phasor measurement at P and Q preceding fault, respectively; $Z_C^{(i)}$ and $\gamma^{(i)}$ are the ith sequence characteristic impedance and propagation constant of the transmission line, respectively. The relationship between $Z_C^{(i)}$, $\gamma^{(i)}$ and $r^{(i)}, x^{(i)}, b^{(i)}$ can be found in [29]. In (5.3) - (5.5), i equals to one, since only positive-sequence quantities exist in normal operation condition.

Substitution of (5.3) and (5.4) into (5.5) leads to

$$\begin{aligned} f_k(X) = &[-\frac{1}{Z_C^{(1)}}\sinh(\gamma^{(1)}l_{PC})V_{0P}^{(1)k} + \cosh(\gamma^{(1)}l_{PC})I_{0P}^{(1)k}] \\ &+[-\frac{1}{Z_C^{(1)}}\sinh(\gamma^{(1)}l_{CQ})V_{0Q}^{(1)k} + \cosh(\gamma^{(1)}l_{CQ})I_{0Q}^{(1)k}] = 0 \end{aligned}, \quad k = 1,\ldots,N \tag{5.6}$$

Based on the equivalent Pi circuit during normal operation as shown in Figure 5.2, another key relationship can be presented as

$$
\begin{aligned}
&V_{0cL}^{(1)k} - I_{0cL}^{(1)k} Z_{SC} - V_{0cR}^{(1)k} \\
&= [\cosh(\gamma^{(i)} l_{PC}) V_P^{(i)} - Z_C^{(i)} \sinh(\gamma^{(i)} l_{PC}) I_P^{(i)}] - I_{0cL}^{(1)k} Z_{SC} \\
&\quad - [\cosh(\gamma^{(i)} l_{CQ}) V_Q^{(i)} - Z_C^{(i)} \sinh(\gamma^{(i)} l_{CQ}) I_Q^{(i)}] \\
&= 0
\end{aligned}
\tag{5.7}
$$

which can yield functions for N sets of measurements as

$$
\begin{aligned}
f_{N+k}(X) = &[\cosh(\gamma^{(i)} l_{PC}) V_P^{(i)} - Z_C^{(i)} \sinh(\gamma^{(i)} l_{PC}) I_P^{(i)}] - I_{0cL}^{(1)k} Z_{SC} \\
&- [\cosh(\gamma^{(i)} l_{CQ}) V_Q^{(i)} - Z_C^{(i)} \sinh(\gamma^{(i)} l_{CQ}) I_Q^{(i)}] = 0
\end{aligned}
, \quad k = 1, \ldots, N \tag{5.8}
$$

The first 2N functions in the function vector can be developed based on (5.6) and (5.8). The other functions are to be constructed based on the during-fault equivalent circuit and corresponding fault type.

If the fault is an AG fault, it holds that

$$
V_f^{(0)} + V_f^{(1)} + V_f^{(2)} = 3R_f I_f^{(1)} \tag{5.9}
$$

where $V_f^{(i)}$ and $I_f^{(i)}$ are the ith sequence fault voltage and current, respectively ($i = 0$ represents zero-sequence, $i = 1$ represents positive-sequence, $i = 2$ represents negative-sequence); R_f is the fault resistance. As R_f is a real number, the term $V_f^{(0)} + V_f^{(1)} + V_f^{(2)}$ are in phase with $I_f^{(1)}$, and such relationship can be represented by the following equation:

$$
f_{2N+1}(X) = \mathrm{Im}\left\{ \frac{V_f^{(1)} + V_f^{(2)} + V_f^{(0)}}{I_f^{(1)}} \right\} = 0 \tag{5.10}
$$

If the fault is a phase B to phase C fault, it holds that

$$V_f^{(1)} - V_f^{(2)} = 3R_f I_f^{(1)} \tag{5.11}$$

Thus, the following function can be obtained:

$$f_{2N+1}(X) = \mathrm{Im}\left\{\frac{V_f^{(1)} - V_f^{(2)}}{I_f^{(1)}}\right\} = 0 \tag{5.12}$$

If the fault is a phase B to phase C to ground fault, it holds that

$$V_f^{(0)} - V_f^{(1)} = -3R_f I_f^{(0)} \tag{5.13}$$

Such equation can be rewritten in the following form:

$$f_{2N+1}(X) = \mathrm{Im}\left\{\frac{V_f^{(0)} - V_f^{(1)}}{I_f^{(0)}}\right\} = 0 \tag{5.14}$$

If the fault is a balanced fault, it holds that

$$V_f^{(1)} = R_f I_f^{(1)} \tag{5.15}$$

Such function can be expressed by

$$f_{2N+1}(X) = \mathrm{Im}\left\{\frac{V_f^{(1)}}{I_f^{(1)}}\right\} = 0 \tag{5.16}$$

The $V_f^{(i)}$ and $I_f^{(i)}$ in (5.10), (5.12), (5.14) and (5.16) can be expressed as functions of the unknown fault location and line parameters based on analysis of the during-fault circuit. It notes that the series compensation device, which is installed at a fixed location along the transmission line, divides the line into two segments. Since on which side the fault occurs is unknown, it is necessary to develop two subroutines addressing possible fault on either side.

5.2.1 Subroutine 1: Fault Occurs To the Left-Hand Side of the Compensator

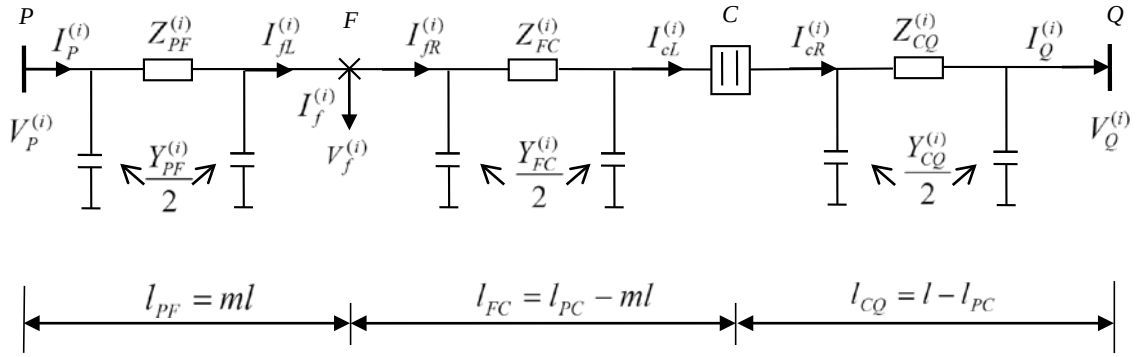

Figure 5.3 The equivalent Pi circuit of *i*th sequence transmission line during fault with a fault to the left of the compensator

The equivalent circuit of *i*th sequence transmission line during the fault is shown in Figure 5.3. Based on the analysis on line segment *PF* in Figure 5.3, the

voltage at the fault point $V_f^{(i)}$ and fault current $I_f^{(i)}$ can be calculated by the following equations:

$$V_f^{(i)} = \cosh(\gamma^{(i)} l_{PF}) V_P^{(i)} - Z_C^{(i)} \sinh(\gamma^{(i)} l_{PF}) I_P^{(i)} \tag{5.17}$$

$$I_f^{(i)} = I_{fL}^{(i)} - I_{fR}^{(i)} \tag{5.18}$$

where $V_P^{(i)}$ and $V_Q^{(i)}$ are the *i*th sequence voltage phasors at *P* and *Q* during fault, respectively ($i = 0,1,2$); $I_P^{(i)}$ and $I_Q^{(i)}$ are the *i*th sequence voltage phasors at *P* and *Q* during fault, respectively ($i = 0,1,2$). $I_{fL}^{(i)}$, the current injection to the fault point from the left-hand-side, can be calculated by the following equation:

$$I_{fL}^{(i)} = -\frac{1}{Z_C^{(i)}} \sinh\left(\gamma^{(i)} l_{PF}\right) V_P^{(i)} + \cosh\left(\gamma^{(i)} l_{PF}\right) I_P^{(i)} \tag{5.19}$$

Another term on the right-hand-side of (5.18), $I_{fR}^{(i)}$, can be derived as follows:

Based on the analysis on the line segment *CQ* in Figure 5.3, the voltage and current to the left side of the compensator can be calculated by the following equation:

$$V_{cL}^{(i)} = V_{cR}^{(i)} + I_{cR}^{(i)} Z_{SC} \tag{5.20}$$

$$I_{cL}^{(i)} = I_{cR}^{(i)} \tag{5.21}$$

where

$$V_{cR}^{(i)} = \cosh(\gamma^{(i)} l_{CQ}) V_Q^{(i)} + Z_C^{(i)} \sinh(\gamma^{(i)} l_{CQ}) I_Q^{(i)} \tag{5.22}$$

$$I_{cR}^{(i)} = \frac{1}{Z_C^{(i)}} \sinh(\gamma^{(i)} l_{CQ}) V_Q^{(i)} + \cosh(\gamma^{(i)} l_{CQ}) I_Q^{(i)} \tag{5.23}$$

Based on the analysis on the segment *FC*, $I_{fR}^{(i)}$ is

$$I_{fR}^{(i)} = \frac{1}{Z_C^{(i)}} \sinh(\gamma^{(i)} l_{FC}) V_{cL}^{(i)} + \cosh(\gamma^{(i)} l_{FC}) I_{cL}^{(i)} \tag{5.24}$$

By substituting (5.20) and (5.21) into (5.24), $I_{fR}^{(i)}$ can be derived, and $I_f^{(i)}$ can be represented by unknown fault distance and line parameters.

Based on the analysis on the segment *FC*, the following equation can be obtained:

$$V_f^{(i)} = \cosh(\gamma^{(i)} l_{FC}) V_{cL}^{(i)} + Z_C^{(i)} \sinh(\gamma^{(i)} l_{FC}) I_{cL}^{(i)} \tag{5.24}$$

By equaling (5.17) and (5.24), another function can be obtained as:

$$\begin{aligned} f_{2N+2}(X) = {} & \cosh(\gamma^{(i)} l_{FC}) V_{cL}^{(i)} + Z_C^{(i)} \sinh(\gamma^{(i)} l_{FC}) I_{cL}^{(i)} \\ & - \left[\cosh(\gamma^{(i)} l_{PF}) V_P^{(i)} - Z_C^{(i)} \sinh(\gamma^{(i)} l_{PF}) I_P^{(i)}\right] = 0 \end{aligned} \tag{5.25}$$

5.2.2 Subroutine 2: Fault Occurs To the Right-Hand Side of the Compensator

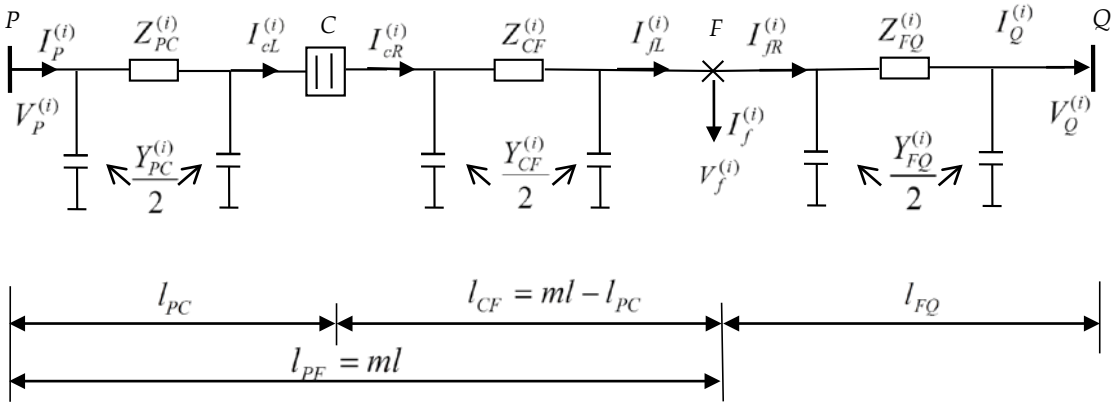

Figure 5.4 The equivalent Pi circuit of ith sequence transmission line during fault with a fault to the right of the compensator

Based on the analysis on the line segment shown in Figure 5.4, the voltage at the fault point $V_f^{(i)}$ and fault current $I_f^{(i)}$ can be calculated by the following equations:

$$V_f^{(i)} = \cosh(\gamma^{(i)} l_{FQ}) V_Q^{(i)} + Z_C^{(i)} \sinh(\gamma^{(i)} l_{FQ}) I_Q^{(i)} \tag{5.26}$$

$$I_f^{(i)} = I_{fL}^{(i)} - I_{fR}^{(i)} \tag{5.27}$$

where

$$I_{fR}^{(i)} = \frac{1}{Z_C^{(i)}} \sinh(\gamma^{(i)} l_{FQ}) V_Q^{(i)} + \cosh(\gamma^{(i)} l_{FQ}) I_Q^{(i)} \tag{5.28}$$

Derivation of $I_{fL}^{(i)}$ is presented as follows:

Based on the analysis on the line segment *PC* in the Figure 5.4, the voltage and current injection on the right side of the series compensator can be calculated as

$$V_{cR}^{(i)} = V_{cL}^{(i)} - I_{cL}^{(i)} Z_{SC} \tag{5.29}$$

$$I_{cR}^{(i)} = I_{cL}^{(i)} \tag{5.30}$$

where

$$V_{cL}^{(i)} = \cosh(\gamma^{(i)} l_{PC}) V_P^{(i)} - Z_C^{(i)} \sinh(\gamma^{(i)} l_{PC}) I_P^{(i)} \tag{5.31}$$

$$I_{cL}^{(i)} = -\frac{1}{Z_C^{(i)}} \sinh(\gamma^{(i)} l_{PC}) V_P^{(i)} + \cosh(\gamma^{(i)} l_{PC}) I_P^{(i)} \tag{5.32}$$

For the line segment *CF* in the Figure 5.4, it holds that

$$I_{fL}^{(i)} = -\frac{1}{Z_C^{(i)}} \sinh(\gamma^{(i)} l_{CF}) V_{cR}^{(i)} + \cosh(\gamma^{(i)} l_{CF}) I_{cR}^{(i)} \tag{5.33}$$

By substituting (5.29) - (5.32) into (5.33), $I_{fL}^{(i)}$ can be derived, and $I_f^{(i)}$ can be represented by unknown fault distance and line parameters.

Based on the analysis on the segment *CF*, the following equation can be obtained:

$$V_f^{(i)} = \cosh(\gamma^{(i)} l_{CF}) V_{cR}^{(i)} - Z_C^{(i)} \sinh(\gamma^{(i)} l_{CF}) I_{cR}^{(i)} \tag{5.34}$$

By equaling (5.26) and (5.34), another function can be obtained as:

$$\begin{aligned} f_{2N+2}(X) = {} & \cosh(\gamma^{(i)} l_{CF}) V_{cR}^{(i)} - Z_C^{(i)} \sinh(\gamma^{(i)} l_{CF}) I_{cR}^{(i)} \\ & - \left[\cosh(\gamma^{(i)} l_{FQ}) V_Q^{(i)} + Z_C^{(i)} \sinh(\gamma^{(i)} l_{FQ}) I_Q^{(i)}\right] = 0 \end{aligned} \tag{5.35}$$

Here concludes the discussion of subroutines.

In summary, the functions are

$$\begin{aligned} f_k(X) = {} & [-\frac{1}{Z_C^{(1)}} \sinh(\gamma^{(1)} l_{PC}) V_{0P}^{(1)k} + \cosh(\gamma^{(1)} l_{PC}) I_{0P}^{(1)k}] \\ & + [-\frac{1}{Z_C^{(1)}} \sinh(\gamma^{(1)} l_{CQ}) V_{0Q}^{(1)k} + \cosh(\gamma^{(1)} l_{CQ}) I_{0Q}^{(1)k}] = 0 \end{aligned} \quad , \quad k = 1, \ldots, N \tag{5.6}$$

$$\begin{aligned} f_{N+k}(X) = {} & [\cosh(\gamma^{(i)} l_{PC}) V_P^{(i)} - Z_C^{(i)} \sinh(\gamma^{(i)} l_{PC}) I_P^{(i)}] - I_{0cL}^{(1)k} Z_{SC} \\ & - [\cosh(\gamma^{(i)} l_{CQ}) V_Q^{(i)} - Z_C^{(i)} \sinh(\gamma^{(i)} l_{CQ}) I_Q^{(i)}] = 0 \end{aligned} \quad , \quad k = 1, \ldots, N \tag{5.8}$$

AG fault $$f_{2N+1}(X) = \mathrm{Im}\left\{\frac{V_f^{(1)} + V_f^{(2)} + V_f^{(0)}}{I_f^{(1)}}\right\} = 0 \tag{5.10}$$

BC fault $$f_{2N+1}(X) = \mathrm{Im}\left\{\frac{V_f^{(1)} - V_f^{(2)}}{I_f^{(1)}}\right\} = 0 \tag{5.12}$$

BCG fault $$f_{2N+1}(X) = \mathrm{Im}\left\{\frac{V_f^{(0)} - V_f^{(1)}}{I_f^{(0)}}\right\} = 0 \tag{5.14}$$

Balanced fault $$f_{2N+1}(X) = \mathrm{Im}\left\{\frac{V_f^{(1)}}{I_f^{(1)}}\right\} = 0 \tag{5.16}$$

Subroutine 1

$$f_{2N+2}(X) = \cosh(\gamma^{(i)} l_{FC}) V_{cL}^{(i)} + Z_C^{(i)} \sinh(\gamma^{(i)} l_{FC}) I_{cL}^{(i)} - \left[\cosh(\gamma^{(i)} l_{PF}) V_P^{(i)} - Z_C^{(i)} \sinh(\gamma^{(i)} l_{PF}) I_P^{(i)}\right] = 0 \quad (5.25)$$

Subroutine 2

$$f_{2N+2}(X) = \cosh(\gamma^{(i)} l_{CF}) V_{cR}^{(i)} - Z_C^{(i)} \sinh(\gamma^{(i)} l_{CF}) I_{cR}^{(i)} - \left[\cosh(\gamma^{(i)} l_{FQ}) V_Q^{(i)} + Z_C^{(i)} \sinh(\gamma^{(i)} l_{FQ}) I_Q^{(i)}\right] = 0 \quad (5.35)$$

Therefore, the function vector $\boldsymbol{F(X)}$ can be obtained as:

$$\boldsymbol{F}_{2i-1}(\boldsymbol{X}) = \mathrm{Re}[f_i(\boldsymbol{X})],\ i = 1,2,...,2N+2 \quad (5.29)$$

$$\boldsymbol{F}_{2i}(\boldsymbol{X}) = \mathrm{Im}[f_i(\boldsymbol{X})],\ i = 1,2,...,2N+2 \quad (5.30)$$

where Re(.) and Im(.) yield the real and imaginary part of their arguments, respectively.

The measurement vector $\boldsymbol{S}$ is formulated as follows:

$$\boldsymbol{S}_i = 0,\ i = 1,2,...,4N+4 \quad (5.33)$$

Note that for balanced faults, only positive-sequence functions should be used, since zero-sequence and negative-sequence quantities do not exist. The measurement vector and function vector are related as

$$\boldsymbol{S} = \boldsymbol{F(X)} + \boldsymbol{\mu} \quad (5.36)$$

where $\boldsymbol{\mu}$ is characterized by the following equation:

$$\boldsymbol{R} = E(\boldsymbol{\mu}\boldsymbol{\mu}^T) \tag{5.37}$$

Elements of $\boldsymbol{R}$ can be specified per the accuracy of meters, and a smaller value indicates a more accurate measurement. The estimate of $\boldsymbol{X}$ can be obtained by minimizing the cost function defined as

$$J = [\boldsymbol{S} - \boldsymbol{F}(\boldsymbol{X})]^T \boldsymbol{R}^{-1} [\boldsymbol{S} - \boldsymbol{F}(\boldsymbol{X})] \tag{5.38}$$

Two fault locations will be derived based on the algorithm presented above. The appropriate estimate can be selected when it satisfies the following principles:

1. The estimated fault location is within the assumed range.
2. The fault resistance calculated based on the estimated fault location is non-negative.
3. X_{SC}, the reactance of the series compensator on each sequence, is negative.

5.3 Evaluation Study

This section presents the simulation results to evaluate the developed fault location algorithm. Matlab SimPowerSystems [68] is used to simulate the series-compensated transmission line and generate voltage and current phasors for faults of different types, locations and resistances. These phasors are fed into the

algorithm to produce the fault location estimate. The initial value for the fault location is chosen as 0.5 p.u. The accuracy of fault location estimate is evaluated by percentage error as defined as the equation (2.39).

The transmission system is studied in per unit system, of which base voltage is 500 kV and base power is 1000 MVA. The bus voltage at bus P is $1.0\angle 20^{\circ}$ p.u., while the bus voltage at bus Q is $1.0\angle 0^{\circ}$ p.u. The positive-sequence source impedance of bus P is (0.0687 + j0.1821) p.u., and its zero-sequence source impedance is (0.0612 + j0.1837) p.u. The positive-sequence source impedance of bus Q is (0.0104 + j0.0589) p.u., and its zero-sequence source impedance is (0.0029 + 0.0605i) p.u. The total length of the studied line is 350 km, and the series compensator is installed 200km away from bus P (0.5714 p.u.). The positive-sequence resistance is 0.0009967 p.u./km, the positive-sequence series reactance is 0.002357 p.u./km, and the positive sequence shunt susceptance is 0.001835 p.u./km. Assume the studied transmission line is compensated with 40% of its total series reactance. Since the positive-sequence total reactance is 0.825 p.u., the series-compensator's reactance on each sequence is -0.33p.u. A value of 1e-6 is chosen for the variance for measurements.

Four representative cases are exhibited as follows:

Case 1: An AG fault occurs at 100 km away from bus P, of which fault resistance is 20 ohm.

The two fault location estimates based on two subroutines are: $m_1 = 0.2861$ and $m_2 = 0.7325$. Based on the first subroutine, the calculated series compensator's reactance is -0.3309 p.u. Based on the second subroutine, the calculated series compensator's reactance is 0.1221 p.u. Therefore, the first estimate is adopted, and it is concluded that the fault location is 0.2861 p.u. from bus *P*. The percentage error of this estimate is 0.15%.

Case 2: A BC fault occurs 260 km away from bus *P*, of which fault resistance is 10 ohm.

The two fault location estimates based on two subroutines are: $m_1 = 0.5932$ and $m_2 = 0.7437$. Since the compensator is installed 0.5714 p.u. from bus *P*, the first estimate is discarded. It is concluded that the fault location is 0.7437 p.u. from bus *P*. The percentage error of this estimate is around 0.11%.

Case 3: A BCG fault occurs at 50 km away from bus *P*, of which fault resistance is 1 ohm.

The two fault location estimates based on two subroutines are: $m_1 = 0.1428$ and $m_2 = 0.6021$. Based on the first subroutine, the calculated series compensator's reactance is -0.3284 p.u. Based on the second subroutine, the calculated series compensator's reactance is 0.0597 p.u. Therefore, the first estimate is adopted, and it is concluded that the fault location is 0.1428 p.u. from bus *P*. The percentage error of this estimate is 0.07%.

Case 4: An ABC fault occurs at 300 km away from bus *P*, of which fault resistance is 5 ohm.

The two fault location estimates based on two subroutines are: $m_1 = 0.7071$ and $m_2 = 0.8587$. Since the compensator is installed 0.5714 p.u. from bus *P*, the first estimate is discarded. It is concluded that the fault location is 0.8587 p.u. from bus *P*. The percentage error of this estimate is around 0.20%.

5.4 Summary

This chapter proposes a parameter-free fault location method for series-compensated transmission lines. Two-terminal voltage and current measurements are utilized. The proposed method does not rely on source impedance.

Based on different fault types, different functions are used. Since the fault location is unknown, two subroutines where fault may occur to either side are considered, and two estimates will be yielded. The true fault location can be determined based on the identification principles.

Evaluation studies based on Matlab SimPowerSystems are implemented, and verify the effectiveness of the proposed fault location method.

Chapter 6 Conclusion

Short-circuit faults may cause severe losses to customers and hazardous impacts on electric power systems. Accurate and prompt fault location can help recover power systems in time, and help avoid potential financial losses and societal disasters.

Compared with conventional fault location methods, the wide-area fault location method proposed in Chapter 2 have several superiorities. It does not rely on local measurements, and can precisely determine fault location with sparse wide-area measurements. Conventional methods assume transmission lines to be always transposed, which may not be true especially in EHV/UHV transmission networks. The proposed method is able to deal with both transposed and untransposed transmission lines. In addition, it is applicable to both single-circuit and double-circuit lines. To fully consider shunt capacitances, distributed parameter line models are used. Moreover, when multiple sets of measurements are available, an optimal estimator can be used to detect and identify potential bad measurements. Also, the system loading conditions do not affect the accuracy of fault location. Evaluation studies on 27-bus, 345kV, 60 Hz transmission network is implemented, and quite accurate fault location estimates can be obtained by the proposed method.

Another key contribution of this dissertation is consideration of complex faults. In Chapter 3, the wide-area fault location method is extended to deal with evolving fault. Evolving faults refers to faults of which fault types change over the fault periods. Fault classification is very challenging for evolving faults. The existing location methods for evolving faults rely on some critical factors, such as extensive amount of training for soft-computing, very high-frequency local measurements, etc. The wide-area fault location method proposed in this dissertation only requires sparse wide-area measurements, and does not need fault type information.

In Chapter 4, fault location method for another complex fault type, inter-circuit fault, is developed. Inter-circuit fault is a type of simultaneous fault, and it is the most common simultaneous fault type. Inter-circuit faults between each circuit in a double-circuit line is the most common inter-circuit fault. Inter-circuit faults can cause serious system instability when phase and ground relaying schemes are used for protection, because they will trip three phases of both circuits. A fault location method for inter-circuit faults on double-circuit lines are developed and evaluated in Chapter 4. Evaluation studies based on EMTP simulation have demonstrated that the proposed algorithms can yield quite accurate estimates under a variety of inter-circuit fault conditions.

The fault location methods proposed in Chapter 2 – Chapter4 require system information such as line parameters. The fault location method proposed in Chapter 5 is a parameter-free method. Neither line parameter information nor the series compensator's capacitance is required. Distributed parameter line model is adopted to fully consider shunt capacitances of long distance lines. Evaluation studies verifies the effectiveness of the fault location method.

REFERENCES

[1] Electricity Training Association, The Institute of Engineering and Technology, *Power System Protection 1: Principles and Components*. London, U.K.: IET, 1995.

[2] H. J. Altuve Ferrer and E. O. Schweitzer, III (eds.), *Modern Solutions for Protection, Control, and Monitoring of Electric Power Systems*. Schweitzer Engineering Laboratories, Inc., Pullman, WA, 2010, pp. 98-99.

[3] M.T. Sant and Y. G. Paithankar, "Online digital fault locator for overhead transmission line," *Electrical Engineers, Proceedings of the Institution of*, vol. 126, no. 11, pp. 1181-1185, Nov. 1979.

[4] M.S Sachdev and R.Agarwal, "A Technique for estimating transmission line fault locations from digital impedance relay measurements," *IEEE Trans. Power Delivery*, vol. 3, no. 1, pp. 121-129, Jan. 1988.

[5] D. Novosel, D. G. Hart, E. Udren, and J. Garitty, "Unsynchronized Two-Terminal Fault Location Estimation," *IEEE Transactions on Power Delivery*, vol. 11, no. 1, pp. 130–138, Jan. 1996.

[6] M. Abe, N. Otsuzuki, T. Emura and M. Takeuchi, "Development of a new fault location system for multi terminal single transmission lines," *Proceedings of IEEE/PES Trans. Distrib. Conf.*, Chicago, IL, 1994, pp. 259-268.

[7] T. Nagasawa, M. Abe, N. Otsuzuki, T. Emura. Y. Jikihara, M. Takeuchi, "Development of a new fault location algorithm for multi-terminal two parallel transmission lines," in *Proceedings of the 1991 IEEE Powe Engineering Society Trans. Distrib. Conf.*, Dallas, TX, 1991, pp. 348-362.

[8] M. Kezunovic and B. Perunicic, "Automated transmission line fault analysis using synchronized sampling at two ends," in *Proceedings Power Industry Computer Applications Conf.*, Salt Lake City, UT, 1995, pp. 407-413.

[9] J.-A. Jiang, J.-Z. Yang, Y.-H. Lin, C.-W. Liu, "An adaptive pmu based fault detection/location technique for transmission lines", *IEEE Trans. Power Del.*, vol. 15, no. 4, pp. 1136-1146, Oct. 2000.

[10] Y. Liao, "Fault location utilizing unsynchronized voltage measurements during fault," *Electric Power Components Systems*, vol. 34, no. 12, pp. 1283-1293, 2006.

[11] Z. Galijasevic and A. Abur, "Fault location using voltage measurements," *IEEE Trans. Power Del.*, vol. 17, no. 2, pp. 441-445, Apr. 2002.

[12] S. M. Brahma, "New fault-location method for a single multi-terminal transmission line using synchronized phasor measurements," *IEEE Trans. Power Del.*, vol. 21, no. 3, pp. 1148-1153, Jul. 2006.

[13] M. Davoudi, J. Sadeh and E. Kanyab, "Parameter-free fault location for transmission lines based on optimisation," *IET Gen. Transm. Distrib.*, vol. 9, no. 11, pp. 1061-1068, 2015.

[14] Y. Liang, G. Wang and H. Li, "Time-domain fault-location method on HVDC transmission lines under unsynchronized two-end measurement and uncertain line parameters," *IEEE Trans. Power Delivery*, vol. 30, no. 3, pp. 1031-1038, 2015.

[15] T. Kawady and J. Stenzel, "A practical fault location approach for double circuit transmission lines using single end data," *IEEE Trans. Power Delivery*, vol. 18, no. 4, pp. 1166-1173, 2003.

[16] Q. Zhang, Y. Zhang, W. Song, Y. Yu, and Z. Wang, "Fault location of two-parallel transmission line for non-earth fault using one-terminal data," *IEEE Trans. Power Delivery*, vol. 14, no. 3, pp. 863-867, 1999.

[17] B. Wang, X. Dong, L. Lan, and F. Xu, "Novel location algorithm for single-line-to-ground faults in transmission line with distributed parameters', *IET Gen., Trans. Distrib.*, vol. 7, no. 6, pp. 560-566, 2013.

[18] A. Salehi-Dobakhshari and A.M.Ranjbar, "Application of synchronised measurements to wide-area diagnosis and location," *IET Gen. Trans. Distrib.*, vol. 8, no. 4, pp. 716-729, 2014.

[19] P. Gopakumar, M.J.B. Reddy and D.K. Mohanta, "Transmission line fault detection and localisation methodology using PMU measurements," *IET Gen. Trans. Distrib.*, vol. 9, no. 11, pp. 1033-1042, 2015.

[20] Y. Liao and S. Elangovan, "Digital distance relaying algorithm for first-zone protection for parallel transmission lines," *Proc. Inst. Elect. Eng. Gen. Transm. Distrib.*, vol. 145, no. 5, pp. 531-536, 1998.

[21] J. Röhrig, "Location of faulty places by measuring with cathode ray oscillograph", *Elektrotech Zeits*, vol. 8, no. 2, pp. 241-242, 1931.

[22] M. H. Idris, M. W. Mustafa, and Y. Yatim, "Effective two terminal single line to ground fault location algorithm", in *2012 IEEE Intl. Power Engineering Opti. Conf.*, Melaka, Malaysia, Jun. 2012.

[23] T. Kawady and J. Stenzel. "Investigation of practical problems for digital fault location algorithms based on EMTP simulation", in *IEEE/PES Transm. Distrib. Conf. Exhibition*, Yokohama, Japan, 2002, pp. 118-123.

[24] M. Dewe, S. Sankar, J. Arrillaga, "The application of satellite time references to hvdc fault location", *IEEE Transactions on Power Delivery*, vol. 8, no. 3, pp. 1295-1302, July 1993.

[25] W. Jin, Y. Lu, and C. Tand, "A novel double ended method for fault location based on traveling-wave time-series," in *IEEE Intl Conf Power System Tech*, Wollongong, Australia, 2016, pp. 1-6.

[26] S. Lin, Z. Y. He, and Q. Q. Qian, "Traveling-wave time-frequency characteristic-based fault location method for transmission lines," *IET Gen. Trans. Distrib.*, vol. 6, no. 8, pp. 764-772, 2012.

[27] *IEEE Standards for Synchrophasor Measurements for Power Systems, IEEE Std C37.117.1-2011*, IEEE Power & Energy Society, 2011.

[28] N. Kang and Y. Liao, "Double-circuit transmission line fault location with the availability of limited voltage measurements," *IEEE Trans. Power Del.*, vol. 27, no. 1, pp. 325-336, Jan. 2012.

[29] J. Grainger and W. Stevenson, *Power System Analysis*. New York: McGraw-Hill, 1994.

[30] M. Korkali, H. Lev-Ari, A. Abur, "Traveling-wave-based fault-location technique for transmission grids via wide-area synchronized voltage measurements," *IEEE Trans. Power Syst.*, vol. 27, no. 1, pp. 1003-1011, 2012.

[31] Q. Jiang, X. Li, B. Wang, *et al.* "PMU-based fault location using voltage measurements in large transmission networks," *IEEE Trans. Power Del.*, vol. 27, no. 1, pp. 1644-1652, 2012.

[32] P. V. Navalkar and S. A. Soman, "Secure remote backup protection of transmission lines using synchrophasors," *IEEE Trans. Power Delivery*, vol. 26, no.1, pp. 87-96, Jan. 2011.

[33] Y. Liao, "A novel method for locating faults on distribution systems," *Electric Power Systems Research Journal*, vol. 117, pp. 21-26, December 2014.

[34] Y. Liao, "Fault location," in *Power Distribution Automation*, London, U.K., The Institute of Engineering and Technology, 2016.

[35] J. C. Li and Y. P. Wu, "A distributed circuit model for three-phase transposed and untransposed transmission lines," *Elect. Power Syst. Res.*, vol. 19, no. 6, pp. 187–194, Oct. 1990.

[36] C. S. Chen, C. W. Liu, and J. A. Jiang, "A new adaptive PMU based protection scheme for transposed/untransposed parallel transmission lines," *IEEE Trans. Power Del.*, vol. 17, no. 2, pp. 395–404, Apr. 2002.

[37] N. D. Tleis, *Power Systems Modelling and Fault Analysis: Theory and Practice*, 7th ed. Oxford, U.K.: Newnes, 2008.

[38] C. A. Apostolopoulos and G. N. Korres, "A novel fault-location algorithm for double-circuit transmission lines without utilizing line parameters," *IEEE Trans. Power Del.*, vol. 26, no. 3, pp. 1467–1478, Jul. 2011.

[39] A. S. Dahane and S. S. Dambhare, "A novel algorithm for differential protection of untransposed transmission line using synchronized measurements," in *11th IET International Conference on Developments in Power Systems Protection (DPSP 2012)*, Birmingham, UK, 2012, pp. 1-4.

[40] *Alternative Transient Program, User Manual and Rule Book*, Leuven EMTP Centre, Leuven, Belgium, 1987.

[41] A. Abur and A. G. Exposito, *Power System State Estimation-Theory and Implementation*. New York: Marcel Dekker, 2004.

[42] Y. Liao and M. Kezunovic, "Optimal estimate of transmission line fault location considering measurement errors," *IEEE Trans. Power Del.*, vol.22, no.3, pp.1335-1341, Jul. 2007

[43] *IEEE Guide For Determining Fault Location On Ac Transmission And Distribution Lines*, IEEE/PES Power System Relaying Committee, 2014.

[44] S. Kulkarni and S. Santoso, "Time-domain algorithm for locating evolving faults," *IEEE Trans. Smart Grid*, vol. 3, no. 4, pp. 1584-1593, 2012.

[45] J. Suonan, Q. Xu, X. Li, S. Liu, and P. Mao, "An evolving fault criterion for UHV transmission line protective relaying," *Proceedings of the CSEE*, vol. 26, no. 4, pp. 93-98, 2006.

[46] D. Costello, "Lessons learned analyzing transmission faults," *SEL Journal Reliable Power*, vol. 1, no. 1, pp. 1-13, 2010.

[47] A. Swetapadma and A. Yadav, "All shunt fault location including cross-country and evolving faults in transmission lines without fault type classification," *Electric Power Systems Research*, 2015, vol. 123, pp. 1-12, 2015.

[48] B. Su, X. Dong, and Y. Sun, "Impact of evolving fault on fault phase selector based on differential superimposed phase currents," *IEEE Power Eng. Soc. Gen. Meeting*, Toronto, Canada, 2003, pp. 2140-2144.

[49] M. Sanaye-Pasand, H. Khorashadi-Zadeh, "Transmission line fault detection & phase selection using ANN," in *Int. Conf. Power System Transients*, New Orleans, LA, USA, Sept.-Oct. 2003, pp. 1-6

[50] Electricity Training Association, The Institute of Engineering and Technology, *Power System Protection 1: Principles and Components*. London, U.K.: IET, 1995.

[51] G. Corpuz, and J. Young, "Case study: analysis of a 138 kV intercircuit fault," in *41st Annu. Western Protective Relay Conf.*, Spokane, WA, 2014, pp. 1-17.

[52] H. J. Altuve Ferrer and E. O. Schweitzer, III (eds.), *Modern Solutions for Protection, Control, and Monitoring of Electric Power Systems*. Pullman, WA: Schweitzer Engineering Laboratories, Inc., 2010, pp. 98-99.

[53] A. Jain, A. S. Thoke, R. N. Patel, and E. Koley, "Intercircuit and cross-country fault detection and classification using artificial neural network," in *2010 Annu. IEEE India Conf.*, Kolkata, India, 2010, pp. 1-4.

[54] V. H. Makwana and B. R. Bhalja, "Digital distance relaying scheme for parallel transmission lines during inter-circuit faults," in *Transmission Line Protection Using Digital Technology*. London, U.K.: Springer-Verlag London Ltd., 2016, pp. 65-88.

[55] E. Hodge and E. Atienza, "Line protection response to a three-phase intercircuit fault," in *42nd Annu. Western Protective Relay Conf.*, Spokane, WA, 2015, pp. 1-6

[56] D. J. Spoor and J. Zhu, "Intercircuit faults and distance relaying of dual-circuit lines," *IEEE Trans. Power Del.*, vol. 20, no. 3, pp. 1846-1852, 2015.

[57] G. Ziegler, Numerical Distance Protection: Principles and Applications. Hoboken, NJ: John Wiley & Sons Inc., 2011.

[58] A. G. Jongepier and V. D. Sluis, "Adaptive distance protection of a double-circuit line," *IEEE Trans. Power Del.*, vol. 9, no. 3, pp. 1289-1297, 1994.

[59] Z. Lu, *et. al.*, "A phase selector based on mathematical morphology for double circuit transmission line," in *Elec. Utility Deregulation Restructuring Power Tech., 2008*, Nanjing, China, 2008, pp. 1-6.

[60] A. Bachmatiuk and J. Izykowski, "Distance protection performance under inter-circuit faults on double-circuit transmission line," *Przeglad Elektrotechniczny*, vol. 89, no. 1, pp. 7-11, 2013.

[61] R. McDaniel, "Analysis of a relay operation for an intercircuit falut," in *68th Annu. Conf. Protective Relay Engineers*, College Station, TX, 2015, pp. 462-477.

[62] M. M. Saha, G. Smetek, and J. Izykowski, "Location of inter-circuit faults on a double-circuit transmission line," in *Modern Elec. Power Systems 2015*, Wrolaw, Poland, 2015, pp. 1-7.

[63] Y. Liao and S. Elangovan, "Unsynchronised two-terminal transmission-line fault-location without using line parameters," *IEE Proceedings - Generation, Transmission and Distribution*, vol. 153, no. 6, pp. 639-643, Nov. 2006.

[64] Y. Liao and N. Kang, "Fault-Location Algorithms Without Utilizing Line Parameters Based on the Distributed Parameter Line Model," I*EEE Trans. Power Del.*, vol. 24, no. 2, pp. 579-584, April 2009.

[65] N. Kang and Y. Liao, "New fault location technique for series compensated transmission line," *International Review of Electrical Engineering*, vol. 2, no. 6, pp. 1385-1390, Dec. 2009.

[66] N. Kang, J. Chen, and Y. Liao, "A fault location algorithm for series-compensated double-circuit transmission lines using distributed parameter line model," *IEEE Trans. Power Del.*, vol. 30, no. 1, pp. 360-367, Feb. 2015.

[67] C. A. Apostolopoulos and G. N. Korres, "A Novel Fault-Location Algorithm for Double-Circuit Transmission Lines Without Utilizing Line Parameters," *IEEE Trans. Power Del.*, vol. 26, no. 3, pp. 1467-1478, July 2011.

[68] *MATLAB SimPowerSystems Help Documentation*. MathWorks Inc., 2009.

VITA

Xiangqing Jiao

Education

2013 – 2017

University of Kentucky, USA, Ph.D. Electrical Engineering

2008 – 2012

Shandong University, China, B.E. Electrical Engineering

Awards

Research Challenge Trust Fellowship, University of Kentucky, USA

Dean's Tuition Scholarship, University of Kentucky, USA

Dean's Commendation for High Achievement, The University of Queensland, Australia

Excellent Student Leader, Shandong University, China

Publications

1. X. Jiao and Y. Liao, "Accurate location of inter-circuit faults on double-circuit transmission lines based on sparse wide-area voltage measurements," in *PES General Meeting 2017*, Chicago, IL, July 2017.

2. X. Jiao and Y. Liao, "Chapter 5 Using PMU measurements for enhanced power grid monitoring and protection," in *Synchronized Phasor Measurements for Smart Grid*, London, U.K., The Institute of Engineering and Technology, 2017.
3. X. Jiao and Y. Liao, "An analytical approach to locate evolving faults on transmission lines based on sparse wide area measurements," in *Power Energy Conference Illinois*, Champaign, IL, Feb. 2017.
4. X. Jiao and Y. Liao, "A linear estimator for transmission line parameters based on distributed parameter line model," in *Power Energy Conference Illinois*, Champaign, IL, Feb. 2017.
5. C. W. Asbery, X. Jiao, and Y. Liao, "Implementation guidance for smart grid communication," in *North American Power Symposium 2016*, Denver, CO, Sept. 2016.
6. X. Jiao and Y. Liao, "Accurate fault location for transposed/untransposed transmission line using sparse wide area measurements," *IEEE Trans. Power Del.*, vol. 31, no.4, pp. 1797-1805, Aug. 2016.
7. Q. Gao and X. Jiao, "Integrated dynamic simulation of PV installations and its low voltage ride through capability analysis," in *Australasian Universities Power Engineering Conference*, Bali, Indonesia, Sept. 2016.